Cu_m/O_2 Bioinorganic Chemistry

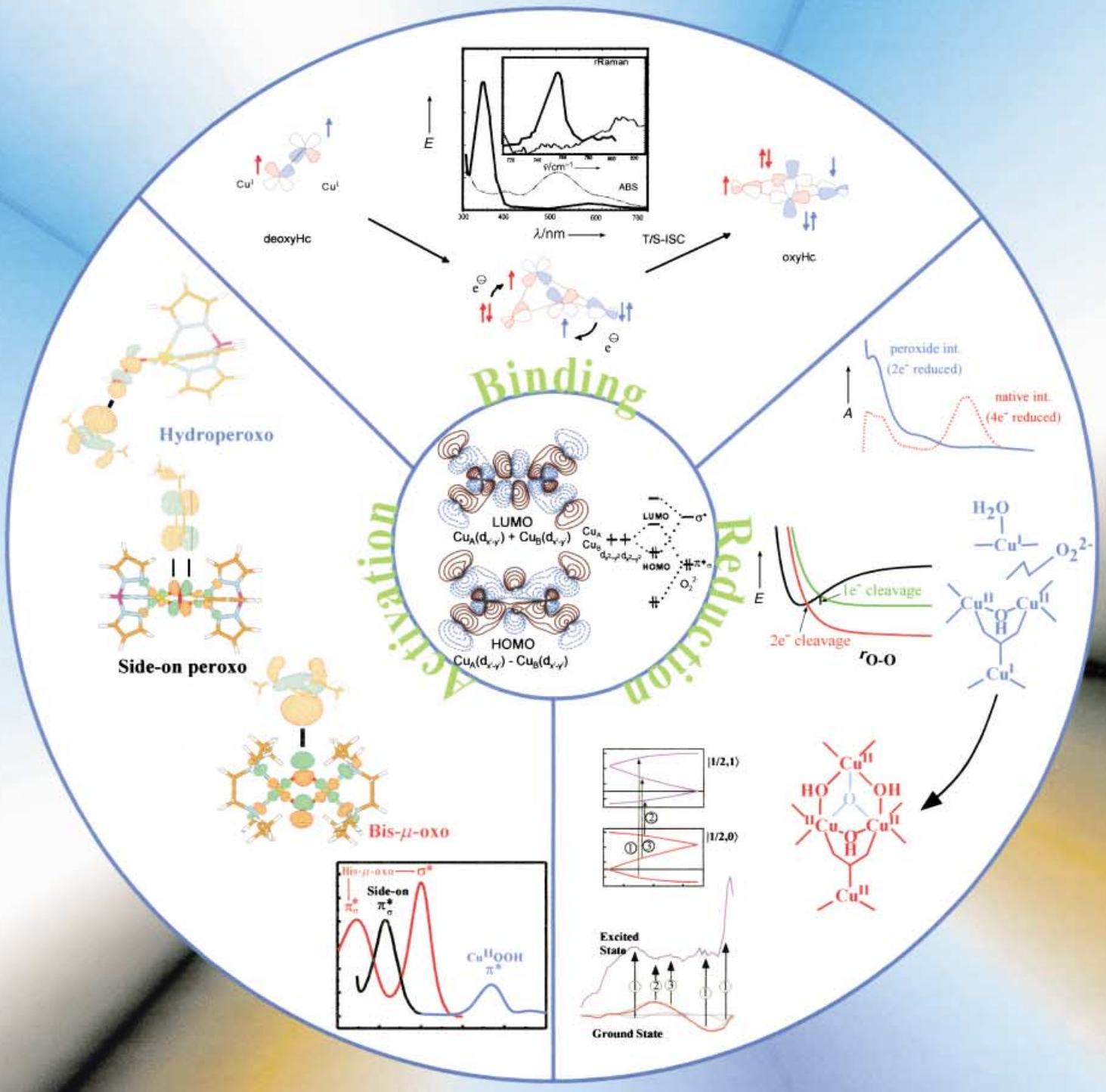

ANGEWANDTE CHEMIE
©WILEY-VCH

Oxygen Binding, Activation, and Reduction to Water by Copper Proteins

Edward I. Solomon,* Peng Chen, Markus Metz, Sang-Kyu Lee, and Amy E. Palmer

Copper active sites play a major role in biological and abiological dioxygen activation. Oxygen intermediates have been studied in detail for the proteins and enzymes involved in reversible O_2 binding (hemocyanin), activation (tyrosinase), and four-electron reduction to water (multicopper oxidases). These oxygen intermediates exhibit unique spectroscopic features indicative of new geometric and electronic structures involved in oxygen activation. The spectroscopic and quantum-mechanical study of these intermediates has defined geometric- and electronic-structure/function correlations, and developed detailed reaction coordinates for the reversible binding of O_2, hydroxylation, and H-atom abstraction from different substrates, and the reductive cleavage of the O–O bond in the formation water.

Keywords: bioinorganic chemistry · copper · electronic structure · metalloenzymes · oxygen activation · reaction mechanisms

1. Introduction

Copper, along with iron active sites dominate the field of biological oxygen chemistry[1] and play important roles in homogeneous[2] and heterogeneous catalysis.[3, 4] Copper proteins are involved in reversible dioxygen binding (hemocyanin),[5] two-electron reduction to peroxide coupled to oxidation of substrates (amine, galactose, and catechol oxidases),[6] activation for hydroxylation (dopamine β-hydroxylase, peptidylglycine α-hydroxylating monooxygenase, tyrosinase, and particulate-methane monooxygenase),[6, 7] and the four-electron reduction to water coupled to substrate oxidation (laccase, ascorbate oxidase, ceruloplasmin and Fet3p)[7] or proton pumping (cytochrome c oxidase, which also contains heme–iron centers).[8] The known copper proteins which are involved in dioxygen binding, activation, and reduction are given in Scheme 1, which is organized based on active-site structural type. Key structural features from the Protein DataBank (PDB) are given in Figure 1.[9–16]

Amine oxidase and galactose oxidase catalyze the two-electron reduction of O_2 to peroxide at a single copper center, which can provide only one electron.[6] As shown in Figure 1A this is accomplished with the aid of an additional redox-active functional group, a topa-quinone in amine oxidase and a tyrosine ligand covalently linked to a cysteine residue through a thioether bond in galactose oxidase. Both functional groups are generated by the post-translational modification of a protein residue by the copper center. In the case of amine oxidase, this involves hydroxylation of a tyrosine by O_2 and involves a single copper center in a reaction that to date is not defined, but may involve tyrosine activation by Cu^{II} centers.[17, 18]

Dopamine β-hydroxylase (DβH) and peptidylglycine α-hydroxylating monooxygenase (PHM) have noncoupled binuclear copper sites,[6] where "coupling" refers to magnetic interactions between the copper centers. This absence of coupling indicates that the Cu^{II} centers of the resting enzyme active site are at least 7 Å apart with no bridging ligation, which is consistent with the crystallographic study on peptidylglycine α-hydroxylating monooxygenase (Figure 1B).[15, 16] The enzyme has one copper center (referred to as Cu_M since it has a methionine ligand[19]) involved in catalysis which is thought to proceed through hydrogen-atom abstraction from the substrate (the benzylic hydrogen in DβH or the α-carbon hydrogen in PHM) by an as-yet unobserved hydroperoxide–Cu^{II}_M complex.[6] The second electron to form the hydroperoxide is derived from Cu_H (the copper with all histidine ligands). Since the copper centers are not coupled (i.e. there is no bridge) the mechanism of transporting the second electron to Cu_M is unclear and has been proposed to involve either a new electron-transfer pathway formed by the substrate bridging the two distant copper centers[16] or by O_2 reduction to superoxide at Cu_H and superoxide channeling to Cu_M.[20]

The coupled binuclear copper proteins include hemocyanin, tyrosinase, and catechol oxidase.[5, 7] The binuclear copper centers in these proteins are strongly coupled through a bridging ligand which provides a direct mechanism for the

[*] Prof. Dr. E. I. Solomon, P. Chen, Dr. M. Metz, Dr. S.-K. Lee, A. E. Palmer
Department of Chemistry
Stanford University
Stanford, CA 94305 (USA)
Fax: (+1) 650-725-0259
E-mail: Edward.Solomon@stanford.edu

 © WILEY-VCH Verlag GmbH, D-69451 Weinheim, 2001 1433-7851/01/4024-4571 $ 17.50+.50/0

two-electron reduction of dioxygen. In oxy-hemocyanin (Figure 1 C) this bridge is the dioxygen unit which binds reversibly to deoxy-hemocyanin ($2\,Cu^{I}$) as peroxide in a side-on bridged (μ-η^2:η^2) structure.[14, 21] This is the most stable oxygen intermediate in copper proteins and exhibits unique spectral features. These features are indicative of a novel electronic structure for the side-on peroxo – Cu^{II}_2 structure which plays a key role in reactivity (Section 2).[5] The spectral/structural features of oxy-hemocyanin and related model complexes provide the reference for oxygen intermediates in the other


E. I. Solomon


P. Chen


M. Metz


A. Palmer


S.-K. Lee

Edward I. Solomon grew up in North Miami Beach, FL, received his Ph.D. from Princeton University (with Donald S. McClure), and was a postdoctoral fellow at the H. C. Ørsted Institute (with Carl J. Ballhausen) and then at Caltech (with Harry B. Gray). He was a professor at MIT until 1982. He then moved to Stanford University where he is now the Monroe E. Spaght Professor of Humanities and Sciences. His research is in the fields of physical-inorganic and bioinorganic chemistry with emphasis on the application of a wide variety of spectroscopic methods to elucidate the electronic structures of transition metal complexes and their contributions to physical properties and reactivity. He has presented numerous named lectures including the First Glen Seaborg Lectures at the University of California, Berkeley, and has been an invited professor at the Tokyo Institute of Technology, Japan, University of Paris, Orsay, France, Tata Institute, Bombay, India, Xiamen University, China, and La Plata University, Argentina. He is a Fellow of the American Academy of Arts and Sciences and the American Association for the Advancement of Sciences and has received a range of awards including the Ira Remsen Award from the Maryland Section of the American Chemical Society, the G. W. Wheland Medal from the University of Chicago and the ACS National Award in Inorganic Chemistry for 2001.

Peng Chen grew up in Jiangsu, China and received his B.S. from Nanjing University in 1997. After spending a year at University of California at San Diego learning organic synthesis with Prof. Yitzhak Tor, he moved to Stanford University where he is the Gerhard Casper Stanford Graduate Fellow working toward his Ph.D. degree in Prof. Edward I. Solomon's group. His research focuses on electronic-structure studies of biologically related copper sites involved in oxygen activation by using a combination of spectroscopic methods and theoretical calculations.

Markus Metz received his Diploma in Chemistry from the Bayerische Julius-Maximilians-Universität Würzburg, Germany, and completed his Ph.D. under the supervision of Prof. Peter Hofmann at he the Ruprecht-Karls-Universität, Heidelberg, on theoretical elucidation of organometallic reaction mechanisms. From 1999 to 2001 he was a DAAD postdoctoral fellow with Professor Edward I. Solomon carrying out theoretical studies on oxygen binding to multinuclear copper proteins. He is a computational chemist at AnorMED Inc. designing metal-based therapeutics.

Amy Palmer received her B.A. in biophysical chemistry in 1994 from Dartmouth College where she studied the molecular mechanism of chromium carcinogenicity with Professor Karen E. Wetterhahn. In 1995, she moved to Stanford University and joined the group of Professor Edward I. Solomon. Her research involves spectroscopic and kinetic studies aimed at elucidating the mechanism of substrate oxidation and O_2 reduction in multicopper enzymes. She is the Franklin Veatch Memorial Fellow at Stanford.

Sang-Kyu Lee, a native of Korea, received his B.S. degree in biochemistry from Lehigh University in 1989 and his Ph.D. degree in biochemistry from the University of Minnesota, Minneapolis, in 1998. His Ph.D studies with Prof. John D. Lipscomb focused on the enzyme reaction mechanism of methane monooxygenase and led to the discovery of reactive intermediates P and Q. He continued his pursuit of metalloprotein enzymology in his postdoctoral research with Prof. Edward I. Solomon through detailed spectroscopic characterization of key intermediates in the reduction of dioxygen to water by multicopper oxidases.

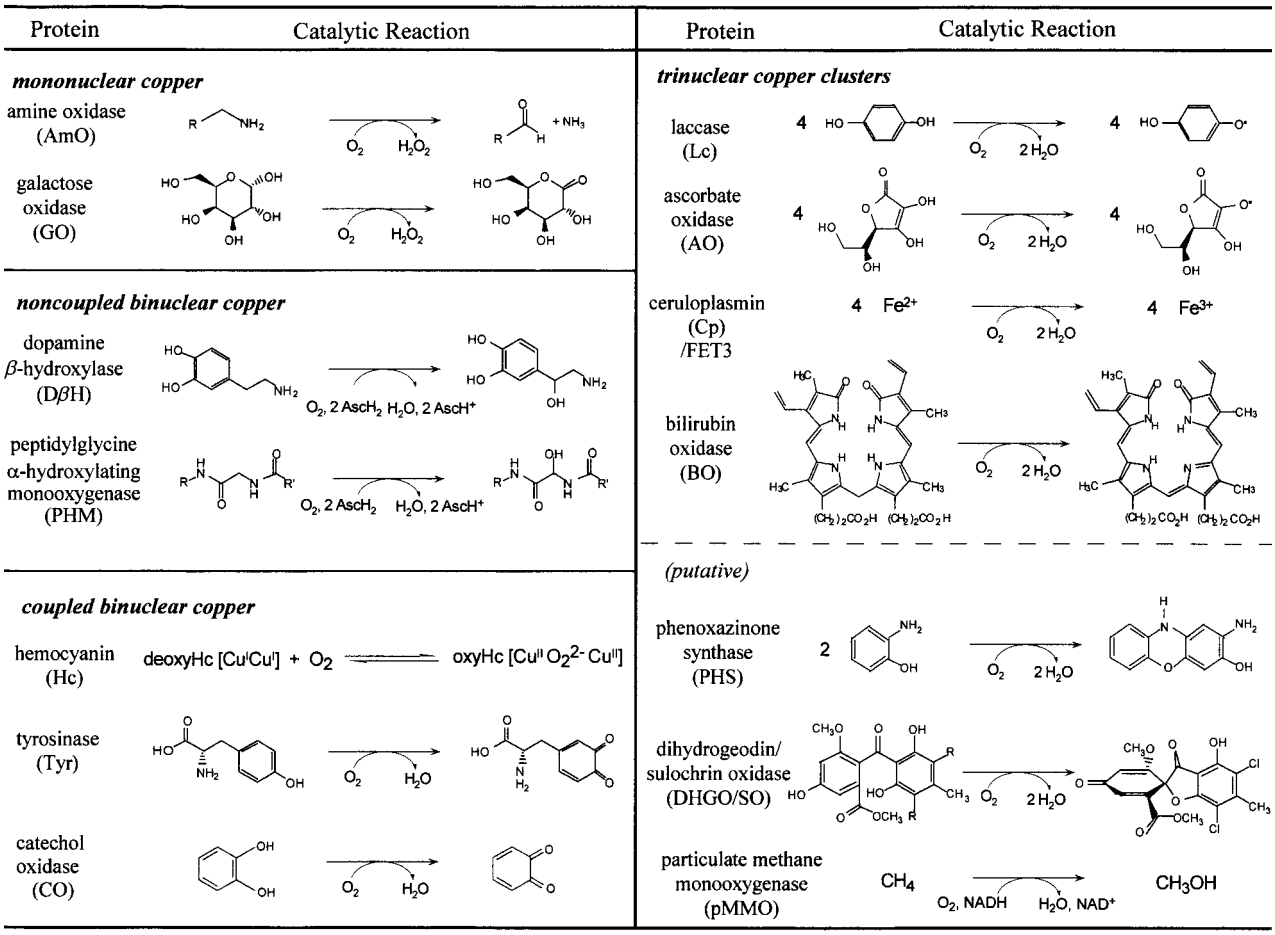

Scheme 1. Copper proteins involved in oxygen binding and activation.

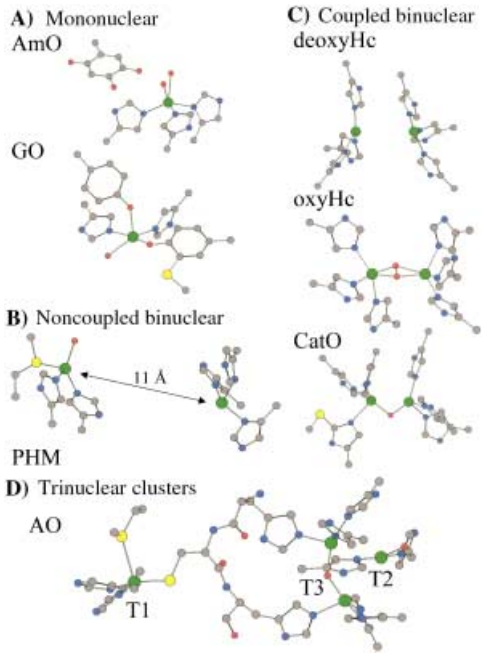

Figure 1. Crystal structures of copper proteins: A) copper amine oxidase (AmO, PDB code *1KSI*), galactose oxidase (GO, PDB code *1GOG*), B) peptidylglycine α-hydroxylating monooxygenase (PHM, PDB code *1PHM*), C) deoxygenated form of hemocyanin (deoxyHc, PDB code *1LLA*), oxygenated form of hemocyanin (oxyHc, PDB code *1OXY*), catechol oxidase (CatO, PDB code *1BT3*), D) ascorbate oxidase (AO, PDB code 1*AOZ*).

copper enzymes which perform different reactions, and allow geometric- and electronic-structure correlations with function in copper chemistry. While a crystal structure is not yet available for tyrosinase, from its spectral features oxy-tyrosinase has a very similar active site to oxy-hemocyanin, the side-on peroxo–Cu_2^{II} structure.[22] However, in the case of oxy-tyrosinase, the site catalyzes the electrophilic oxygenation of phenol to catechol and the two-electron oxidation of catechol to quinone. We have shown that an important difference between hemocyanin and tyrosinase is that the substrate can access and directly coordinate to the copper active site in tyrosinase but not in hemocyanin.[22] The generally accepted mechanism for this reaction is shown in Figure 2.[7] An important question in the monophenolase cycle is whether the side-on bridged peroxo form directly hydroxylates the phenol or whether a bis-μ-oxo Cu_2^{III} structure is also present which carries out this reaction. The side-on peroxo/bis-μ-oxo isomerization was observed and studied in detail in Cu_2O_2 model chemistry.[23] The electronic structures of the side-on peroxo–Cu_2^{II},[24] the bis-μ-oxo Cu_2^{III},[25] and the Cu^{II}–hydroperoxo intermediate[26] indicated above for the noncoupled binuclear copper enzymes will be described and correlated with electrophilic hydroxylation and hydrogen-atom abstraction reactivity in Section 3. The diphenolase mechanism in Figure 2 has been supported by the recent crystal structure of the met (i.e. oxidized, $2\,Cu^{II}$) or resting form of catechol oxidase.[10] The crystal structure also supports

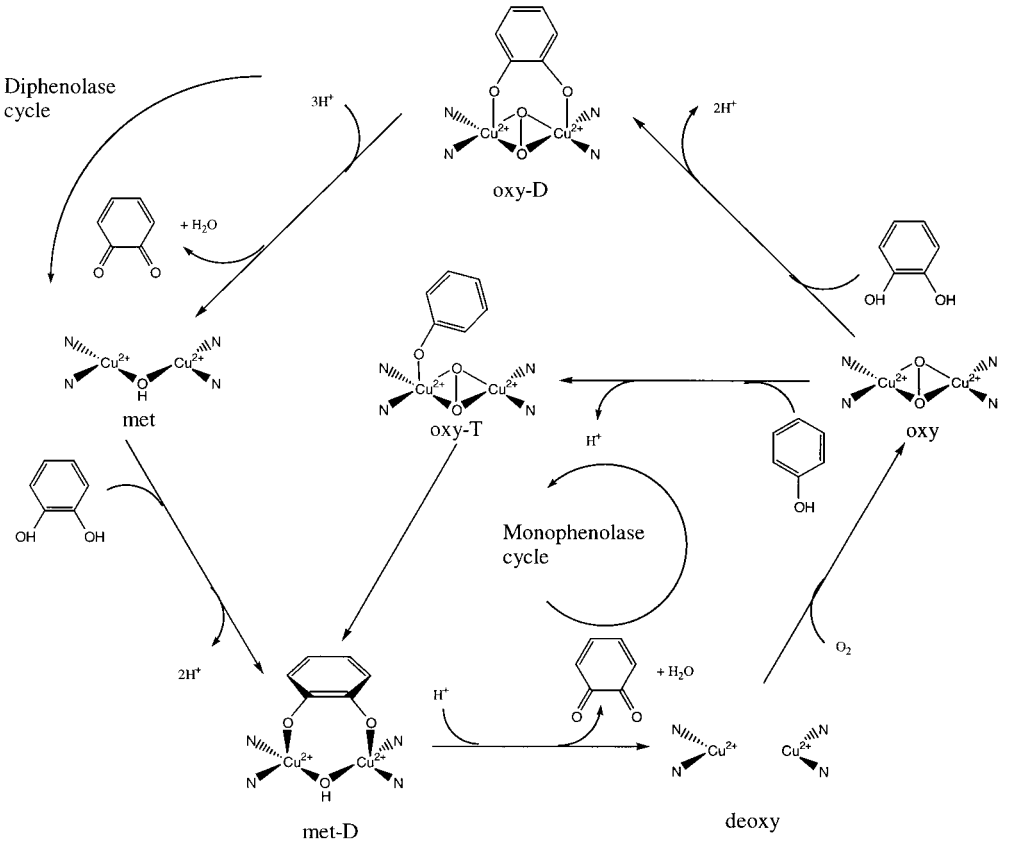

Figure 2. Molecular mechanism for catalysis by tyrosinase. For clarity, the axial ligand on each copper is not included. Reproduced from ref. [27].

the idea of substrate access and coordination to the copper center in catechol oxidase and tyrosinase but not hemocyanin. While both enzymes oxidize catechol to quinone only tyrosinase can hydroxylate phenol. The structural origin of this difference in reactivity is not yet clear but may relate to different structural requirements for the different reactions. Spectral data on the binding of competitive inhibitors to the binuclear Cu site in tyrosinase indicate that a trigonal-bipyramidal rearrangement is involved in phenol hydroxylation (monophenolase cycle, oxy-T $\rightarrow$met-D, Figure 2) but not catechol oxidation (diphenolase cycle).[27]

The final class of structural types in biological Cu/O_2 chemistry is the trinuclear copper cluster found in the multicopper oxidases[7, 28] and potentially in other enzymes including particulate-methane monooxygenase.[29] Laccase and Fet3p[30] are the simplest of the multicopper oxidases. These enzymes contain a trinuclear copper cluster (comprising a hydroxide-bridged coupled binuclear Cu^{II} center called type 3, T3[31] and a three-coordinate mononuclear Cu^{II} center called type 2, T2) and an additional blue, or type 1 (T1), copper center. The type 1 Cu center is >13 Å from the trinuclear cluster but linked to it through an electron-transfer pathway (T1 – Cys – His – T3) (Figure 1D).[9] Ascorbate oxidase is basically a dimer of laccase, and ceruloplasmin contains two additional remote type 1 copper centers.[9, 32] Substrate oxidation occurs at the type 1 center and electrons are transferred rapidly over the >13 Å electron-transfer pathway to the trinuclear copper cluster where dioxygen is reduced to water. An oxygen intermediate, known as the native intermediate, is trapped in the reduction of O_2 by fully reduced (i.e. $4Cu^{I}$) laccase.[7, 33–35] If the type 1 center is replaced by a redox-inactive mercuric ion[36] (the T1Hg derivative) and the reduced trinuclear copper cluster is treated with O_2, a less-reduced oxygen intermediate, the peroxide intermediate, is generated.[37] These intermediates have been studied in detail and this has led to the molecular mechanism for the four-electron reduction of dioxygen to water and a general model for the reductive cleavage of the O–O bond.[38] These studies are presented in Section 4.

The research described below demonstrates the power of combining spectroscopy with density functional theory (DFT) in developing geometric- and electronic-structure/function correlations in biological systems.

2. Dioxygen Binding

2.1. Unique Electronic Structure of Oxy-Hemocyanin

As indicated in the introduction, oxy-hemocyanin and structurally equivalent μ-η^2:η^2 side-on peroxo-bridged binuclear copper model complexes exhibit unique spectral features.[1, 5, 7, 39] First consider peroxide end-on bound in a mononuclear tetragonal Cu^{II} complex as a reference. The key valence orbitals are the high-energy, half-occupied $d_{x^2-y^2}$ orbital on the copper center and the doubly degenerate π^* HOMO on the peroxide.[5] As shown in Figure 3A, one π^* orbital will form a σ bond with the Cu $d_{x^2-y^2}$ orbital and be stabilized (the π^*_σ) whereby the $d_{x^2-y^2}$ half-occupied HOMO will be destabilized, while the other π^* orbital is perpendicular to the Cu-O-O plane (the π^*_v, v = vertical) and only weakly interacts with the copper center. As charge-transfer absorption intensity reflects orbital overlap, the peroxide σ-donor bond produces one intense charge-transfer (CT) transition, the peroxo $\pi^*_\sigma \rightarrow$Cu $d_{x^2-y^2}$ charge transfer. This transfer is observed experimentally in an end-on bound peroxo – Cu^{II} model complex as an absorption band at around 500 nm with $\varepsilon \approx 5800\,M^{-1}cm^{-1}$ (Figure 3B).[40] Also included in Figure 3B is the absorption spectrum of oxy-hemocyanin which exhibits the peroxide $\pi^*_\sigma \rightarrow Cu^{II}$ charge-transfer transition at much higher energy and with about four times the intensity ($\lambda = 350$ nm, $\varepsilon \sim 20000\,M^{-1}cm^{-1}$).[40, 41] Resonance Raman spectra obtained by excitation into these peroxide

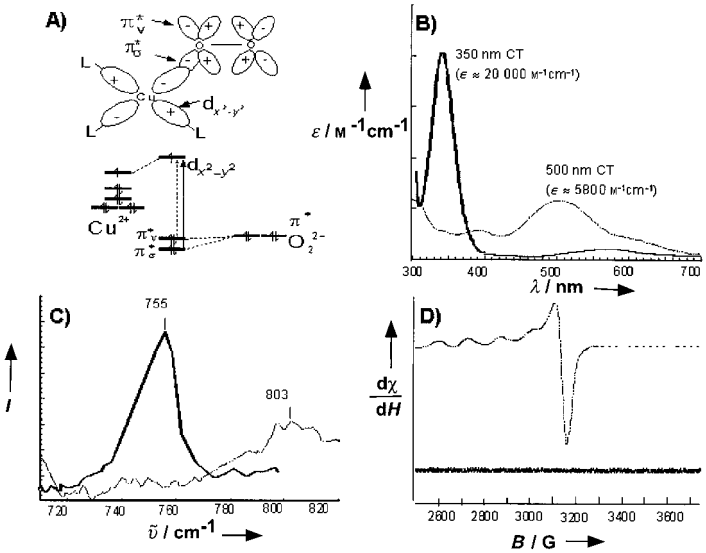

Figure 3. A) Electronic structure of the peroxide – Cu^{II} bond of an end-on bound peroxy – Cu^{II} model complex. Adapted from ref. [5], B) absorption spectra of oxy-hemocyanin (——) and a peroxy – Cu^{II} model complex (- - - -); CT = charge transfer, C) resonance Raman spectra of the intra-peroxide stretch of oxy-hemocyanin (——) and the peroxy – Cu^{II} model complex (——), D) EPR spectra of the oxy-hemocyanin (lower spectrum) and of a tetragonal Cu^{II} model complex. Adapted from ref. [7].

charge-transfer transitions (Figure 3C) show an O–O stretch at about 800 cm^{-1} for the end-on bound peroxide – Cu^{II} model complex, while for oxy-hemocyanin this vibration is at 750 cm^{-1} reflecting an extremely weak O–O bond.[40, 42] Finally, in contrast to mononuclear tetragonal Cu^{II} complexes which exhibit the "normal" EPR spectrum shown in Figure 3D, oxy-hemocyanin has no EPR signal because of the magnetic coupling between the two Cu^{II} centers, mediated by the peroxide bridge.[7] From SQUID (superconducting quantum-interference device) magnetic susceptibility measurements there is a strong antiferromagnetic coupling (two Cu^{II} centers with $S = ½$ couple to form a singlet and a triplet) with the singlet ground state below the triplet by more than 600 cm^{-1}.[43]

We have shown that these unique spectral features reflect the novel electronic structure of the side-on peroxo-bridged Cu_2^{II} complex in Figure 1C.[24, 44] As shown in Figure 4, the HOMO and LUMO for the binuclear Cu^{II} complexes are formed if one takes the symmetric and antisymmetric linear combinations of the half occupied $d_{x^2-y^2}$ orbitals of the two copper centers and allows these to interact with the peroxide valence orbitals in the side-on structure. The dominant interaction again involves the π_σ^* orbital and its bonding with the symmetric combination of $d_{x^2-y^2}$ orbitals to form the LUMO. As with the end-on bound peroxo – Cu^{II} complex in Figure 3A a peroxide σ-donor bond is formed, however, the bonding/antibonding interaction is much larger. The origin of this strong σ-donor interaction can be observed in the contours of the LUMO, where, in the side-on bridged structure, the peroxide has four σ-donor bonds to the two copper centers. This very strong σ-donor interaction leads to the high energy of the peroxide $\pi_\sigma^* \rightarrow Cu^{II}$ charge-transfer transition of oxy-hemocyanin and to its high intensity which reflects the orbital overlap and hence the strength of the σ-donation. An additional bonding interaction is observed in oxy-hemocyanin which is not present in the end-on peroxo – Cu^{II} monomer. This interaction involves stabilization of the antisymmetric combination of $d_{x^2-y^2}$ orbitals by a small bonding interaction with the high-energy unoccupied σ* orbital on the peroxide (Figure 4, HOMO contour). This in turn leads to some π backbonding of electron density from the copper center into the σ* orbital of the peroxide, which is strongly antibonding with respect to the O–O bond. This leads to a very weak peroxide bond and the low O–O stretching frequency in the resonance Raman spectrum of oxy-hemocyanin (Figure 3C).[45] Finally, since in dimers the bridging ligand causes the HOMO/LUMO splitting which is the origin of the antiferromagnetic coupling, the combination of very strong σ donation (destabilization of the LUMO) and π backbonding (stabilization of the HOMO) leads to the large stabilization of the singlet ground state in oxy-hemocyanin.[24]

From the bonding description of oxy-hemocyanin (Figure 4) the key occupied valence orbitals (peroxide π_σ^* and the HOMO ($d_{x^2-y^2} - d_{x^2-y^2}$)) are lowered in energy which gives a very strong peroxide – Cu_2^{II} bond. This stabilizes oxy-hemocyanin from loss of peroxide, which would produce an oxidized (i.e. met) site which can no longer function in dioxygen binding, and greatly contributes to the energetics of O_2 binding to hemocyanin as presented in Section 2.2.

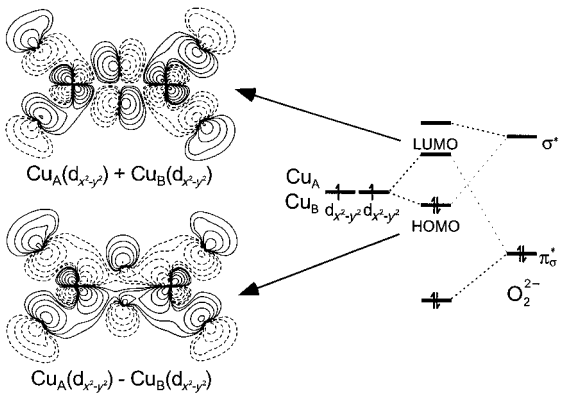

Figure 4. Electronic structure of the peroxide – Cu^{II} bond of oxy-hemocyanin. Adapted from ref. [1].

2.2. The Reaction Coordinate

The unique spectral features for oxy-hemocyanin described above and the more limited data available for deoxy-hemocyanin (two Cu^{I} centers with d^{10} configurations) have been used to evaluate and calibrate hybrid-DFT calculations (at the B3LYP/Lanl2dz level)[46–50] which include time-dependent DFT[51, 52] to correlate to spectral data. These results will not be discussed here except to indicate that the calculations of structural and spectroscopic data and the general bonding description obtained are reasonable, but the oxy-hemocyanin site is calculated to be too covalent and this will effect energetic considerations (see below).[53] These calculations give the change in electronic structure on O_2 binding to deoxy-hemocyanin (Figure 5). The HOMO of

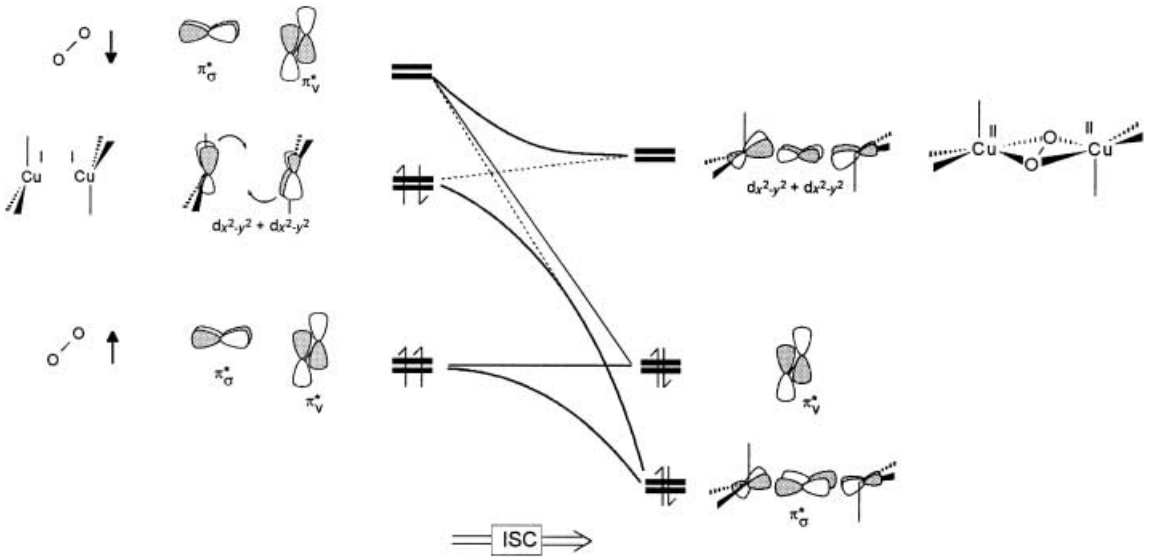

Figure 5. Orbital correlation diagram for O_2 binding to deoxy-hemocyanin. Adapted from ref. [53].

deoxy-hemocyanin has $d_{x^2-y^2}$ orbitals perpendicular to the Cu–Cu vector (each copper(I) unit has an approximately trigonal-planar structure). On O_2 binding these $d_{x^2-y^2}$ orbitals are destabilized and rotate to donate two electrons into the π^* orbital set of O_2 reducing the dioxygen to peroxide and producing the copper-centered LUMO (Figure 5, right, and Figure 4).[53] Thus, O_2 binding involves two-electron transfer and intersystem crossing (ISC) from triplet dioxygen to the singlet ground state of oxy-hemocyanin.

We have used these experimentally calibrated electronic-structure calculations to evaluate the reaction coordinate of oxygen binding to hemocyanin.[53] Figure 6 shows the structures obtained as the peroxide of oxy-hemocyanin is displaced

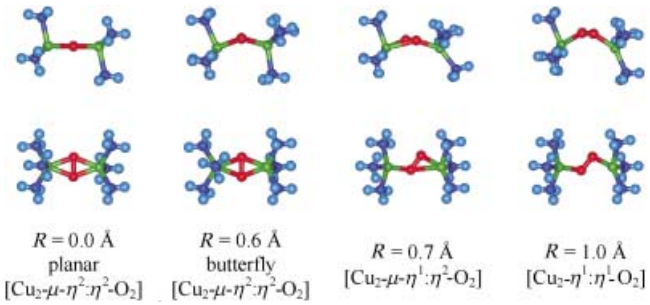

Figure 6. The reaction coordinate of O_2 coordination/release by Hemocyanin. Top: view along the O–O bond in $[Cu_2(\mu\text{-}\eta^2\text{:}\eta^2O_2)]$; Bottom: molecules rotated around the copper – copper vector by 90°. Adapted from ref. [53].

by an amount R above the molecular plane and the geometry is partially optimized on going to the deoxy site with O_2 release. First, the site distorts to a butterfly structure, then to an asymmetrically bridged $\mu\text{-}\eta^1\text{:}\eta^2$, then to an end-on bridged $\mu\text{-}\eta^1\text{:}\eta^1$ structure, and finally loss of O_2 (not shown in Figure 6). This reaction coordinate reflects that maximizing metal – ligand overlap plays a dominant role in determining the coordination mode and shows that even though a nonsymmetric coordination mode does occur, it is energetically favorable to bridge the two copper centers of the binuclear active site.

Figure 7 presents the change in charge along this reaction coordinate. As the peroxide is displaced from the molecular plane, the positive charge on the copper center and the

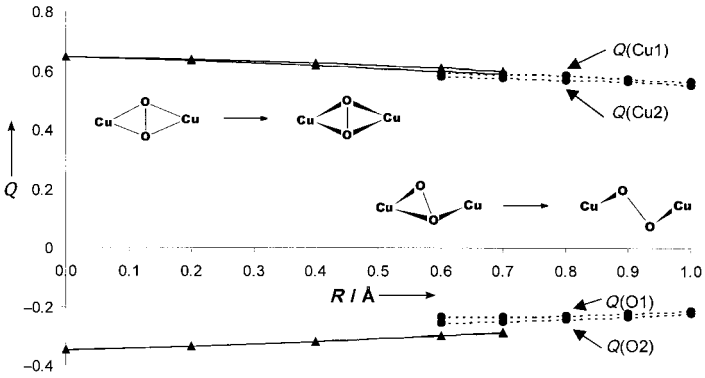

Figure 7. Changes of partial charges (Q) of the copper and oxygen atoms during O_2 release from oxy-hemocyanin in the singlet state with $\mu\text{-}\eta^2\text{:}\eta^2\text{-}O_2$ coordination (——) and in the triplet state with nonsymmetric O_2 coordination (- - - -). R is the distance between the center of the O – O and Cu – Cu vectors. Adapted from ref. [53].

negative charge on the peroxide oxygen atoms continually decrease, consistent with charge transfer to form dioxygen and the reduced site. The charge is donated equivalently to both copper centers even in the non-symmetric $\mu\text{-}\eta^1\text{:}\eta^2$ coordination mode. Thus, simultaneous two-electron transfer is thermodynamically favorable for the peroxide-bridged binuclear copper site. The continuous charge flow in the singlet state prepares the complex for ISC.

We have been particularly interested in understanding how hemocyanin overcomes the spin-forbidden O_2 binding.[53] Figure 8 shows that along the reaction coordinate for O_2 release, as the peroxide is raised above the molecular plane in the butterfly distorted structure the singlet/triplet splitting

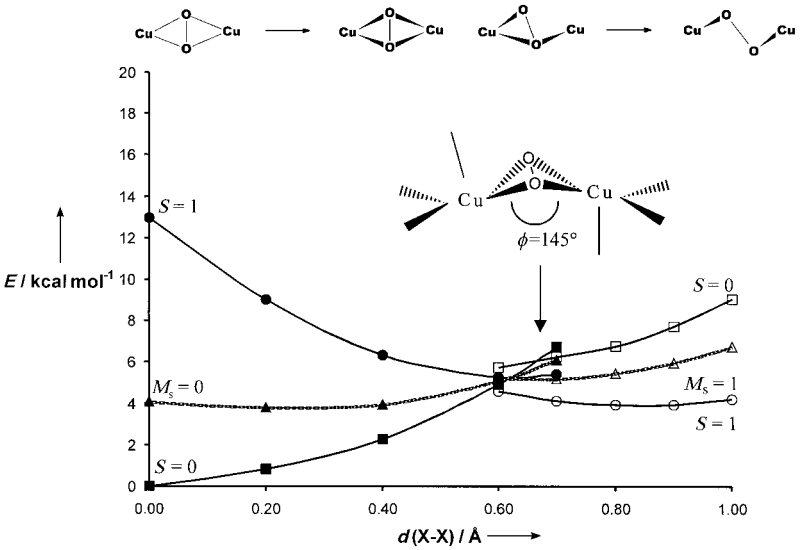

Figure 8. Potential-energy surfaces for the interconversion of oxy-hemocyanin and deoxy-hemocyanin. Filled patterns: symmetric O_2 coordination (μ-η^2:η^2); open patterns: non-symmetric O_2 coordination (μ-η^1:η^2 and μ-η^2:η^2); triplet state: $S=1$; broken symmetry state: magnetic spin quantum number $M_s=0$; singlet state ($S=0$) is spin-projected. The term d(X-X) is the distance between the center of the O–O and the Cu–Cu vectors. Adapted from ref. [53].

greatly decreases and there is ISC at $R \sim 0.6$ Å. As the peroxide is displaced out of the Cu_2O_2 plane, the π^*_σ becomes less σ bonding and the π^*_v becomes involved in σ overlap. These events bring the π* set of orbitals on the peroxide bridge energetically close together and allows them to orient along individual Cu-$\eta^2O_2^{2-}$ planes (Figure 9). As shown in Figure 9B, this produces close to an orthogonal magnetic-orbital pathway between the two Cu^{II} centers which eliminates the superexchange coupling and leads to the triplet ground state. The reduced antiferromagnetic interaction is also apparent from the small contribution of the second copper center to the LUMO (Figure 9B). From Scheme 2 for the triplet ground state, electron transfer results in a spin-up electron in each orthogonal π* orbital of the peroxide which correlates with the $^3\Sigma_g^-$ ground state of O_2 and leads to further energetic stabilization of the triplet ground state by single-center electron exchange.

The energetics of O_2 binding to deoxy-hemocyanin are summarized in Figure 10 and compared to those of mononuclear Cu model systems. The O_2 binding is found to be exothermic by about 16 kcal mol^{-1} which is approximately twice that determined by experiment and reflects that the B3LYP/Lanl2dz calculations overestimate the covalency of the bonds in oxy-hemocyanin. The calculations reproduce the change in energy of O_2 binding observed between the tense and the relaxed quaternary structures of hemocyanin,[1, 54] where the relaxed deoxy site has a shorter Cu^I–Cu^I distance (3.5 Å vs. 4.6 Å for the tense site) and a higher affinity for O_2.[14] Importantly, the calculations show that O_2 binding to isolated Cu^I monomers to form the μ-η^2:η^2 $O_2^{2-}Cu^{II}_2$ dimer is less favorable, which reflects that the protein destabilizes the deoxy site by holding the two Cu^I centers only a short distance apart. This proximity produces a repulsive interaction and increases the exothermicity of O_2 binding to the binuclear copper site in the protein and also provides a mechanism for the protein to regulate the O_2 affinity (i.e. cooperativity) by changing the Cu–Cu distance in deoxy-hemocyanin.[53] (In model complexes this reaction is made more favorable by strained multidentate ligands which destabilize the Cu^I site.[55, 56])

In summary (Figure 11), when triplet O_2 binds to deoxy-hemocyanin, charge is transferred from the copper centers which shifts the unpaired spin density onto the separate metal centers reducing the exchange stabilization of the $^3\Sigma_g^-$ ground state of dioxygen. The reaction coordinate then turns on the superexchange pathway through the bridging peroxide which leads to antiferromagnetic coupling and thus stabilization of the singlet state. This appears to be a general mechanism utilized to overcome the spin-forbidden O_2 binding by coupled binuclear metal sites in metalloproteins.[53]

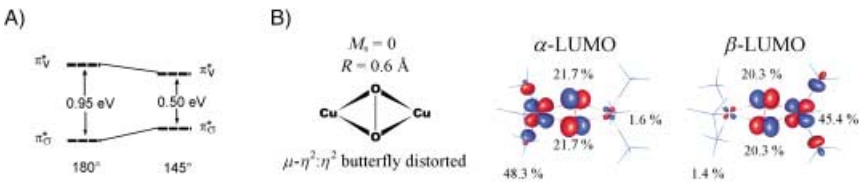

Figure 9. A) Reduction of the energy difference between the two π* peroxide orbitals from butterfly distortion of the [Cu_2(μ-η^2:η^2O_2)] core (spin-orbital energies are averaged), B) contour surface plots of the α and β LUMO obtained from broken-symmetry calculations on the butterfly structure (Figure 8). The Cu and O orbital contributions are obtained from Mulliken population analysis. Adapted from ref. [53].

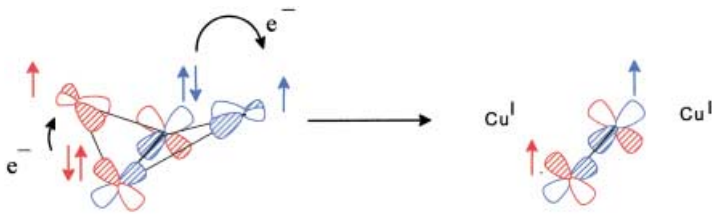

Scheme 2. Electron transfer out of orthogonal π* peroxide orbitals in the triplet state. Adapted from ref. [53].

3. O_2 Activation by Copper Enzymes and Related Model Complexes

As presented in the introduction, a mononuclear Cu^{II}–hydroperoxide complex (Scheme 3A) is thought to be the catalytic intermediate in H-atom abstraction from substrates in the noncoupled binuclear copper enzymes DβH and PHM.[6] In the coupled binuclear copper enzyme tyrosinase which catalyzes the electrophilic hydroxylation of phenol (Figure 2), a side-on peroxide-bridged

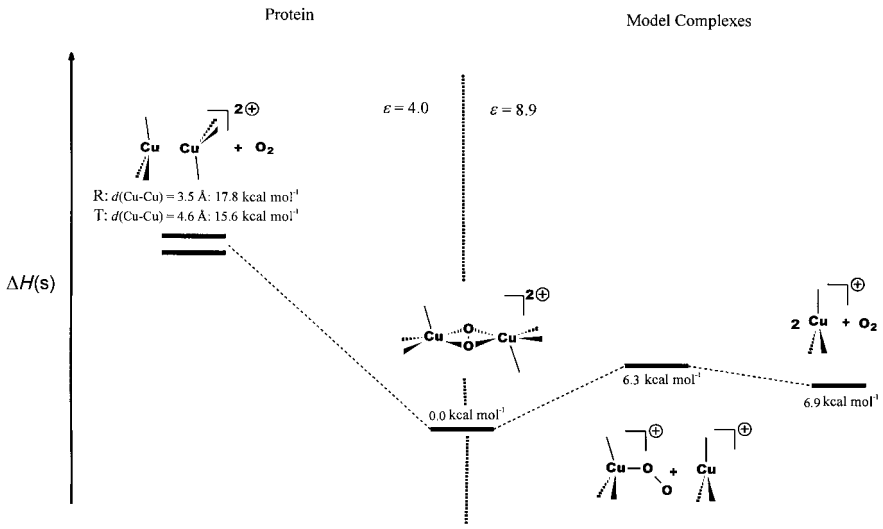

Figure 10. Energy minima of the binuclear (left: protein) and mononuclear model complexes (right) at different stages of O_2 reduction. A mononuclear superoxo complex is included which is not found for the binuclear models. Energy values are derived from spin-projection, frequency, and PCM (polarized continuum model) calculations. For clarity the NH_3 ligands are indicated by lines; R = relaxed structure, T = tense structure, ε = dielectric constant. Adapted from ref. [53].

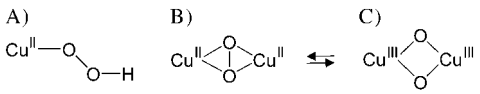

Scheme 3. Key Cu/O_2 species involved in the dioxygen activation.

binuclear Cu_2^{II} intermediate equivalent to oxy-hemocyanin is present (Scheme 3B).[7] In copper model complexes this side-on peroxo–Cu_2^{II} structure can be in rapid equilibrium with the bis-μ-oxo Cu_2^{III} isomer (Scheme 3C).[23] As presented in section 2.1 for the side-on peroxo–Cu_2^{II} structure, we have used spectroscopy combined with DFT calculations to elucidate the electronic structures of the three peroxo species in Scheme 3.[24–26] Here we consider how these electronic structures contribute to peroxide activation for electrophilic hydroxylation and H-atom abstraction and define electronic differences related to differences in reactivity.

We first consider the binuclear Cu–XYL model system $[Cu_2^I(NO_2\text{-XYL})]$ from Karlin et al (Scheme 4; XYL = *N*,*N*,*N*′,*N*′-tetra(2-pyridylethyl)-3,5-di-(aminomethyl)phenyl) which has been shown to hydroxylate the aromatic ring of the ligand through an electrophilic mechanism very similar to that of tyrosinase.[57] At low temperature with an electron withdrawing $R = NO_2$ group on the ring *para* to the position being hydroxylated, the oxygen intermediate can be stabilized; its absorption spectrum (Figure 12A) is very similar to that of the side-on peroxide-bridged Cu_2^{II} site of oxy-hemocyanin and oxy-tyrosinase but with an additional feature at around 430 nm (ca. 25250 cm^{-1}) which could be contributed by bis-μ-oxo Cu_2^{III} isomer. This possibility could be evaluated experimentally through resonance Raman spectroscopy of this band (Figure 12B).[58] The bis-μ-oxo Cu_2^{III} species would

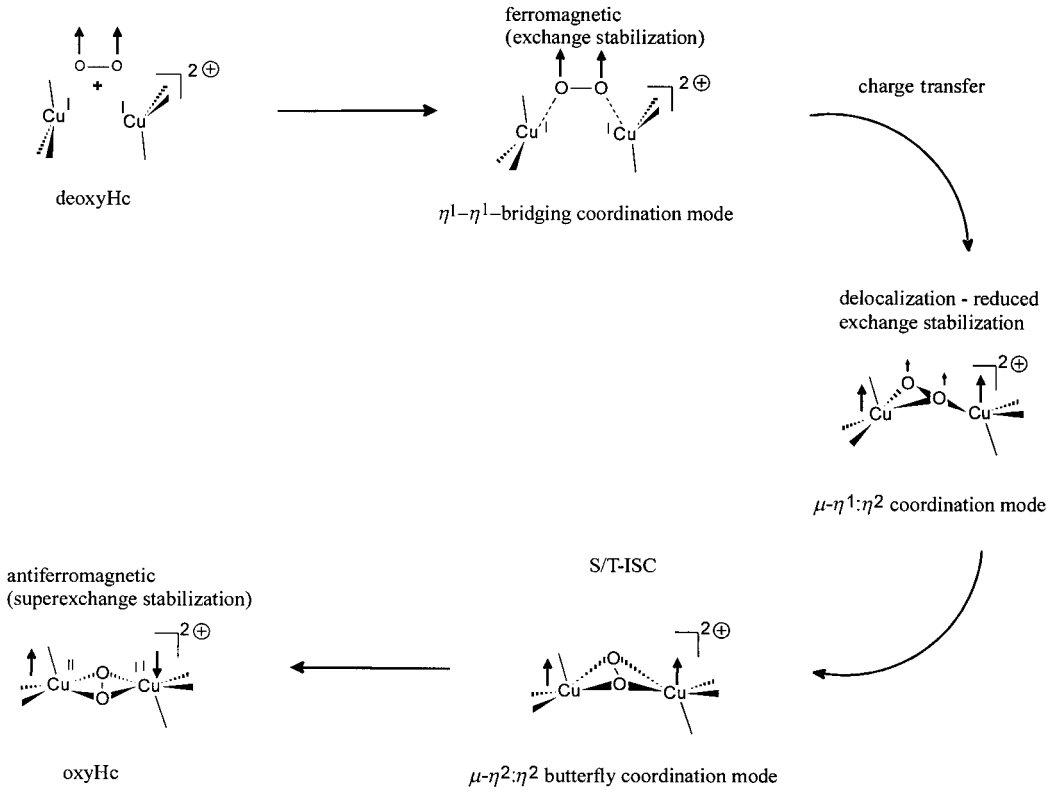

Figure 11. Illustration of the relevant steps for O_2 binding to deoxy-hemocyanin. Localization of unpaired electrons is indicated by arrows (up:α; down:β); S/T-ISC = singlet/triplet intersystem crossing. Adapted from ref. [53].

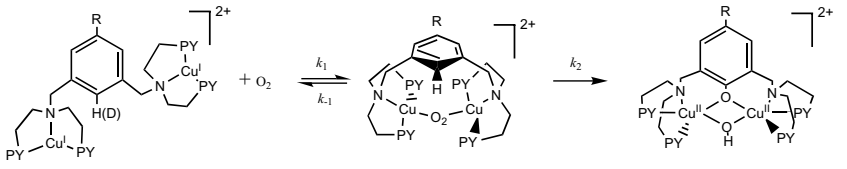

Scheme 4. Electrophilic aromatic hydroxylation reaction, PY = pyridinyl. Reproduced from ref. [58].

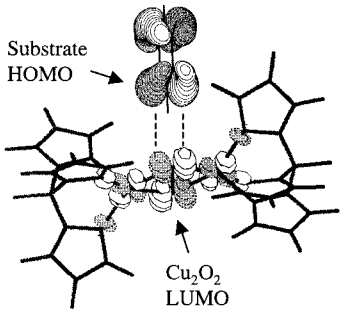

Figure 13. Frontier molecular orbitals showing π overlap of the benzene HOMO and side-on bridged μ-η^2:η^2 peroxo–Cu_2^{II} LUMO. The side-on complex is modeled by the $[Cu_2(HBPz_3)_2](O_2)$ molecule in the DFT calculation; HBPz3 = hydrotris(3,5-dialkyl-1-pyrazolyl)borate.

exhibit an intense Cu_2O_2 core vibration at approximately 600 cm^{-1} which is not present in Figure 12B, which indicates that the absorption band at about 400 nm is in fact associated with the side-on peroxo–Cu_2^{II} structure and is derived from a butterfly distortion of the $Cu_2(O_2)$ core.[59] From the noise level of the Raman spectrum (Figure 12B) an upper limit of $<0.1\,\%$ can be determined for the amount of this bis-μ-oxo Cu_2^{III} species present in the Cu–XYL system.

The side-on peroxo species has a O–O vibration at 747 cm^{-1} which was used to monitor the time course of the hydroxylation reaction. From Figures 12C and D the ν(O–O) band disappears as the ν(C–O) band associated with the hydroxylated ring grows. Thus, either the side-on peroxo directly hydroxylates the ring or it is in a rapid equilibrium with the bis-μ-oxo structure. But as the bis-μ-oxo structure is present at $<0.1\,\%$, this species would have to be several orders of magnitude more reactive than the side-on peroxo species, for it to be responsible for the hydroxylation.

The relative reactivities of the side-on peroxo, bis-μ-oxo, and Cu^{II}-OOH structures (Scheme 3) could be evaluated using frontier molecular orbital (FMO) theory.[25, 26, 58] As shown in Figure 13 an electrophilic mechanism involves the interaction of the HOMO of the donor substrate with the LUMO of the acceptor which in the Cu–XYL case is the Cu_2O_2 core.[58] Electrophilic attack on the aromatic ring of the XYL model complex in Scheme 4 requires good π overlap of the valence orbitals. This in turn requires oxygen π character in the LUMO of the metal site. As shown in Figure 4 and described in Section 2.1 for the side-on peroxo core, π character in the LUMO is derived from the strong donor interaction of the peroxide π_σ^* orbital with the $d_{x^2-y^2}$ derived LUMO of the copper center (Figure 14, middle). The lower the energy of the LUMO and higher the coefficient of mixing of the peroxide π_σ^* orbital into this LUMO the greater the activation for aromatic electrophilic hydroxylation. The energy and π_σ^* character of this orbital is directly reflected in the energy and intensity, respectively, of the O_2^{2-} $\pi_\sigma^* \rightarrow Cu^{II}$ charge-transfer transition as discussed in Section 2.1 for the side-on peroxo structure and included in Figure 15. We have performed equivalent spectroscopic/electronic-structure

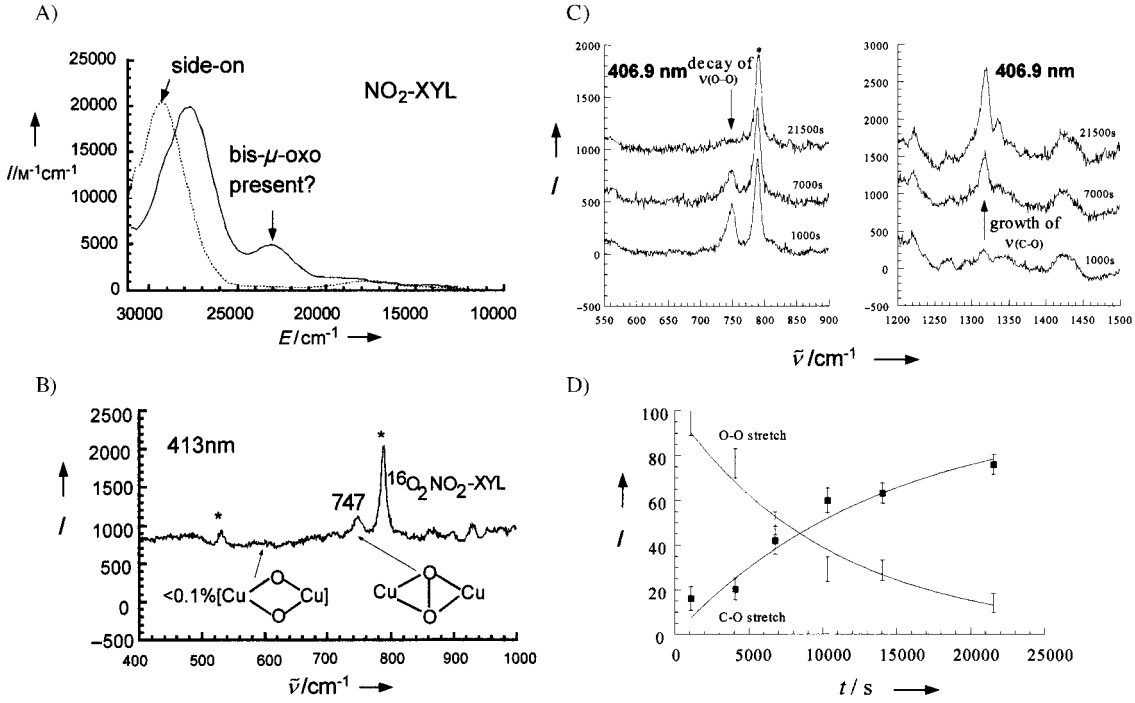

Figure 12. A) Absorption spectra of $[Cu_2(NO_2\text{-XYL})(O_2)]^{2+}$ and the side-on bridged μ-η^2:η^2 peroxo–Cu_2^{II} models, B) resonance Raman spectrum of $[Cu_2(NO_2\text{-XYL})(O_2)]^{2+}$ excited at 413 nm, C) time dependence of resonance Raman signals of $[Cu_2(NO_2\text{-XYL})(O_2)]^{2+}$ ions during the hydroxylation reaction. D) Correlation of O–O and C–O vibrations in the resonance Raman spectra of $[Cu_2(NO_2\text{-XYL})(O_2)]^{2+}$ ions. Reproduced from ref. [58].

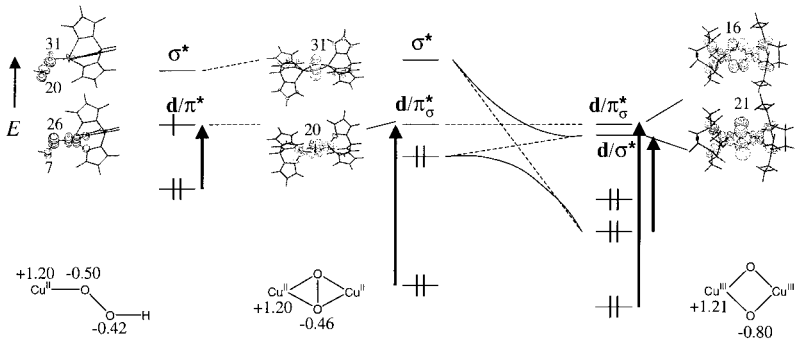

Figure 14. Valence molecular-orbital energy diagrams of copper hydroperoxo, side-on peroxo, and bis-μ-oxo species. Atomic contributions are labeled next to individual MOs (upper). Atom charges are labeled on the chemical structure (lower). Molecular orbitals are labeled by their dominant fragment contributions, thus, d/π^* is a copper d-based orbital with a significant peroxide π^* contribution. The model complexes used are $[Cu(HBPz_3)(OOH)]$, $[Cu_2(HBPz_3)_2(O_2)]$, and $[(L_{ME})_2Cu_2O_2]^{2+}$; $L_{ME} = N,N'$-dimethyl-N,N'-diethylcyclohexyldiamine.

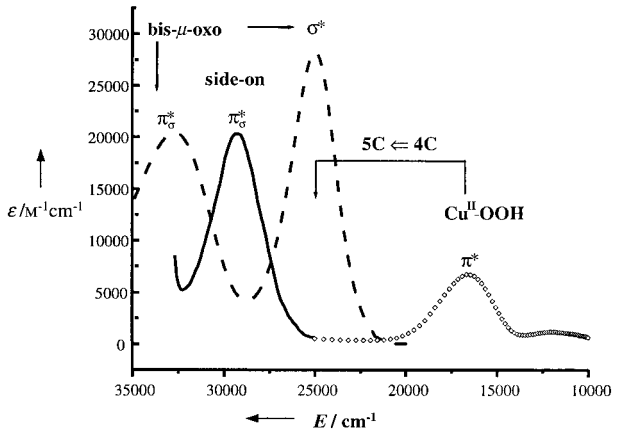

Figure 15. Absorption spectra of side-on peroxo – Cu_2^{II}, bis-μ-oxo Cu_2^{III}, and hydroperoxo – Cu^{II} complexes. Note that the spectrum for the hydroperoxo – Cu^{II} complex is that of a four-coordinate species while the other species are five coordinate. Charge-transfer transitions blue shift by around 8000 – 10000 cm^{-1} in changing from four coordinate to five coordinate as indicated by the arrow for the hydroperoxo – Cu^{II} complex.

studies on the Cu^{II} – hydroperoxide[26] and bis-μ-oxo Cu_2^{III} structures[25] in model complexes leading to the electronic structures at the left and right, respectively, in Figure 14. Their charge-transfer absorption spectra are included in Figure 15. For equivalent ligation, the energies of the LUMOs of all three species are similar. However, for the hydroperoxide – Cu^{II} complex the LUMO contains very little π^* character on the noncoordinated oxygen that would be available for attack on the substrate. Thus, the hydroperoxide – Cu^{II} species should not be effective for electrophilic π attack on aromatic substrates (Figure 16). Alternatively, both the side-on peroxo and the bis-μ-oxo structures have similar π^*_σ peroxide character in their LUMOs and should be similarly activated for electrophilic aromatic hydroxylation. However, in frontier molecular orbital theory there is also a charge term and since the oxygen of the bis-μ-oxo structure are more negative (i.e. more oxide character) this would disfavor the bis-μ-oxo structure relative to the side-on peroxo structure in aromatic hydroxylation (Figure 16). Thus, for the Karlin Cu – XYL system, it is clear that the side-on peroxo-bridged Cu_2^{II} species is responsible for the aromatic hydroxylation. Its concentration is greater than that of the bis-μ-oxo species by more than three orders magnitude and it should be more reactive because of the difference in charge on the oxygen atom. These studies are now being extended to oxy-tyrosinase to determine whether substrate coordination affects the nature of the oxygen species involved in the hydroxylation of the phenol ring.

Figure 14 shows that there is an additional electronic pathway for electrophilic attack on substrates by these copper – oxygen species involving the LUMO+1. Protonation of the peroxide in Cu^{II} – OOH and the large charge donation to the copper centers in the side-on peroxo structure greatly lower the energy of the peroxide σ^* orbital.[26, 60] This reduction in energy leads to the backbonding in the side-on peroxo structure (see Section 2.1). In the bis-μ-oxo species the backbonding cleaves the O–O bond and the σ^* orbital is dramatically lowered in energy to correlate with the LUMO which contains significant σ^* character.[25] This effect can be observed in the charge-transfer spectra of the bis-μ-oxo species (Figure 15) where the new intense low-energy band at $\sim$25000 cm^{-1} reflects the σ^* character in the LUMO. The σ^* pathway (Figure 17) requires good σ overlap with substrates and would be active in reactions, for example, involving oxo transfer to the electron lone pair on a phosphane. From Figure 17 it can be seen that both the hydroperoxide – Cu^{II} and side-on peroxo-bridged Cu_2^{II} species are activated to a similar extent for a σ electrophilic attack, as is observed experimentally.[26, 61]

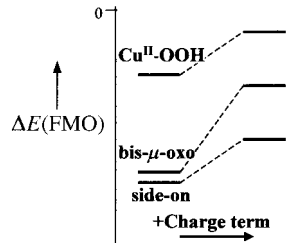

Figure 16. Qualitative frontier molecular-orbital analysis of relative reactivities (more negative ΔE = more reactive) of the different Cu/O_2 species in terms of π^* electrophilic attack (left, the FMO term; right, with inclusion of charge term).

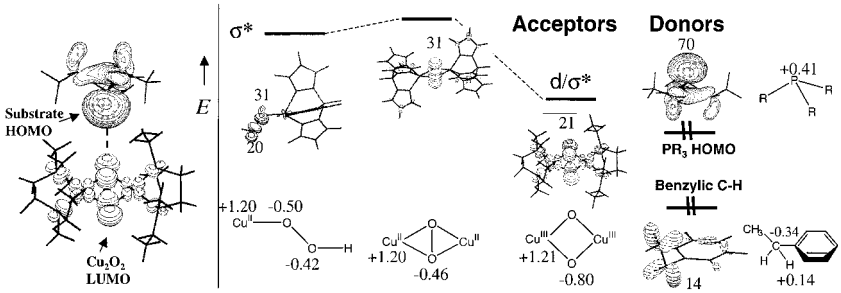

Figure 17. Left: Frontier molecular orbitals indicating σ overlap of the phosphane HOMO and bis-μ-oxo Cu^{III}_2 LUMO. Right: Valence molecular orbital energy diagrams of Cu hydroperoxo, side-on peroxo, and bis-μ-oxo species, and relevant substrates showing the σ^* pathway. Atomic contributions are labeled next to individual MOs. Atom charges are labeled on the chemical structure.

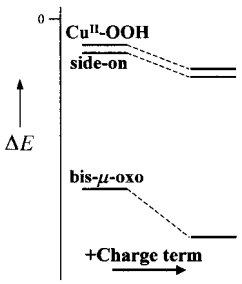

Figure 18. Qualitative frontier molecular-orbital analysis of relative reactivities of different Cu/O_2 species in terms of σ* electrophilic attack (left, the FMO term; right, with inclusion of charge term).

The low energy of the σ*-containing LUMO of the bis-μ-oxo Cu_2^{III} structure makes electrophilic attack more favorable. This effect is further enhanced (Figure 18) by the charge term as the P atom in PR_3 has partial positive character. Comparison of Figure 17 with Figure 18 indicates a large difference in the electrophilic reactivity of these copper–oxygen species for σ- versus π-donor substrates.[62]

Steric factors would limit the σ interaction of bulky substrates with the compact bis-μ-oxo Cu_2^{III} core.[62] However, this would be less of a limitation for H-atom abstraction which would involve the same σ-LUMO pathways shown in Figure 17, thus predicting parallel reactivities for the different copper–oxygen species (Figure 18). The bis-μ-oxo would be most effective as it has the lowest lying σ* LUMO and the most favorable charge term. From frontier molecular orbital theory, the side-on peroxo species should be less active, and there should be a large additional Franck–Condon activation barrier associated with the one-electron reductive cleavage of the O–O bond (Figure 19, considered further in section 4.2.3).[25] Finally H-atom abstraction by the Cu^{II}–OOH species is found to be energetically unfavorable (Figure 20 A).[26] This situation results from the fact that a Cu^{II}–oxyl species would be produced which would only be stabilized by one π-bonding interaction between the Cu and the O centers (see LUMO in Figure 20 B). Thus, for Dβ H and PHM either there is further stabilization of the Cu^{II}–oxyl/Cu^{III}–oxo intermediate which could arise from the complex geometry or the presence of the methionine ligand on Cu_M, or an alternative mechanism for the hydroxylation of the substrates by these enzymes is operative. These possibilities are now being evaluated.

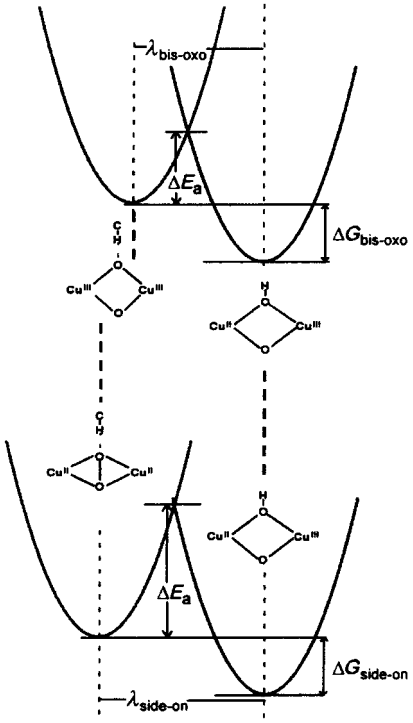

Figure 19. Representation of Franck–Condon barriers of bis-μ-oxo (top) and side-on peroxo (bottom) species for H-atom abstraction; λ = geometric distortion. Adapted from ref. [25].

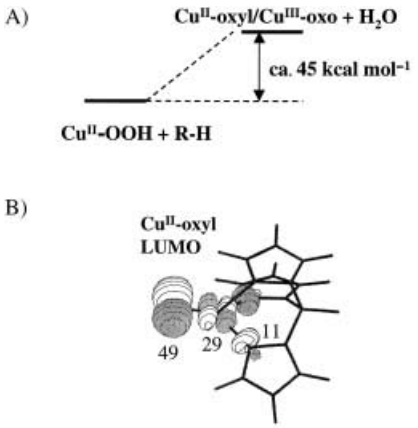

	Cu	Pz^{ax}	O	OH	Pz^{eq} × 2	BH
Cu^{II}-OOH	1.20	−0.41	**−0.51**	0	−0.37	0.44
Cu^{II}-oxyl	1.25	−0.40	**−0.64**	-	−0.33	0.44
Cu^{II}-oxide	0.79	−0.45	**−0.83**	-	−0.45	0.38

Figure 20. A) Calculated energy change for the H-atom abstraction by Cu^{II}OOH, B) B3LYP calculated LUMO of formally Cu^{II}–oxyl species formed by H-atom abstraction. Atomic contributions are labeled. Table gives calculated atom charges *Q* for relevant species. In the calculation the Cu^{II}–oxyl was modeled by the [Cu(HBPz$_3$)]–oxyl complex.

4. O_2 Reduction to H_2O

4.1. The Trinuclear Copper-Cluster Active Site

As indicated in the introduction, the multicopper oxidases contain three types of copper (types 1–3) with type 3 being a coupled binuclear copper pair.[7] In our early studies we demonstrated that the type 2 and type 3 centers form a trinuclear copper cluster which plays a key role in the reduction of dioxygen to water by the multicopper oxidases.[63, 64] This result has now been strongly supported by X-ray crystallography for the three multicopper oxidases, fungal laccase,[65] ceruloplasmin,[32] and ascorbate oxidase.[9] These studies further showed that the distant type 1 Cu center is linked to the trinuclear copper cluster through the Cys–His electron-transfer pathway (Figure 1 D). The T1Hg derivative,[36] where the type 1 copper is replaced by the redox and spectroscopically inactive mercury ion, has allowed the results from spectroscopy to be correlated with those from crystallography to gain an insight into the electronic structure of the trinuclear copper-cluster site.[66] Low-temperature magnetic circular dichroism (MCD) spectroscopy is sensitive to paramagnetic centers, thus it can selectively probe the ligand-field

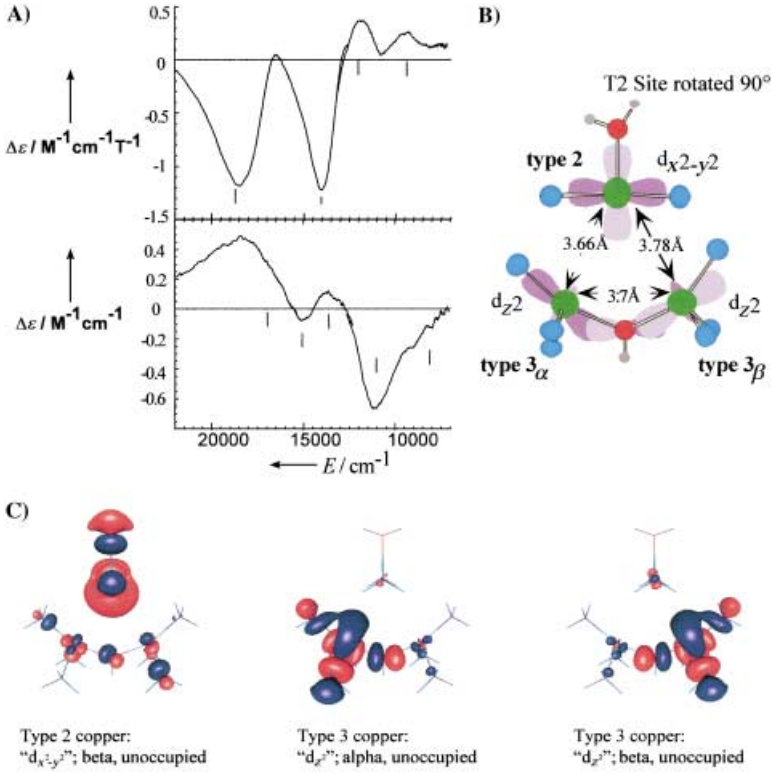

Figure 21. A) Ligand-field transitions (energies indicated by vertical lines) of the trinuclear cluster (top: low-temperature MCD depicts the type 2 Cu transitions, bottom: room-temperature CD depicts the type 3 Cu transitions). Note that there are more than four ligand-field transitions in the CD spectrum indicating that the two type 3 Cu centers are inequivalent, B) ligand-field derived electronic structure of the trinuclear cluster. The HOMO of each Cu center is displayed. Reproduced from ref. [67], C) surface plots of unoccupied MOs obtained from unrestricted DFT calculations. Superposition of these MOs is consistent with the ligand-field result presented in (B) with additional 4p mixing along the coordinatively unsaturated positions of each type 3 copper center.

transitions of the type 2 copper centers ($S = ½$; Figure 21 A, top). Reduction of the type 2 center in the T1Hg derivative results in no change in the circular dichroism (CD) spectrum indicating that the spectral features observed in CD (Figure 21 A, bottom) are ligand-field transitions of the two oxidized type 3 copper centers. These transitions are relatively intense in absorption/CD spectrum because of the distorted geometry of the type 3 copper (see below) but do not contribute to the low-temperature MCD spectrum as these copper centers are magnetically coupled to produce a diamagnetic $S = 0$ ground state. Through ligand-field calculations, the transition energies in Figure 21 A give the description of the electronic structure of the trinuclear copper cluster in Figure 21 B.[67] The three-coordinate type 2 copper center (2 His, 1 H_2O ligand) has a $d_{x^2-y^2}$ ground state and has a square-planar copper environment with an open coordination position oriented toward the two type 3 copper centers. Whereas the type 3 copper centers are four-coordinate (3 His, 1 μ-OH ligand), their electronic structures can best be described as trigonal bipyramidal with open coordination positions in their equatorial planes oriented toward the type 2 copper. Both type 3 copper centers have d_{z^2} ground states, which are oriented for strong antiferromagnetic coupling through the bridging OH^- ion. Thus, the trinuclear copper cluster is ideally configured to react with dioxygen to generate bridged intermediates. Recent DFT calculations support this description (Figure 21 C). Note that these are spin-unrestricted broken-symmetry calculations where the three unoccupied orbitals pictured together reflect the spin distributions on the three copper centers of the trimer, that is, the two T3 Cu centers are antiferromagnetically coupled and the T2 Cu center only weakly interacts with them. In addition, these calculations show 4p mixing for the two type 3 copper centers along the coordinatively unsaturated positions, which could make an important contribution to ligand binding. As with hemocyanin (Section 2.2), one role of the protein is to hold the copper centers of the cluster together which leads to repulsive interactions that would stabilize anionic oxygen intermediates binding within the cluster.[68]

4.2. O_2 Reduction

Reaction of fully reduced native laccase (reduced type 1, reduced trinuclear cluster) and the fully reduced T1Hg laccase derivative (reduced trinuclear cluster) with dioxygen produces different intermediates, namely the native and T1Hg intermediate, respectively, with the absorption spectra given in Figure 22 A.[35, 37, 69, 70] The native enzyme, in contrast to the T1Hg derivative, has a redox-active type 1 center which is oxidized in this reaction (the type 1 absorption band at about 600 nm grows at the same rate as the feature at

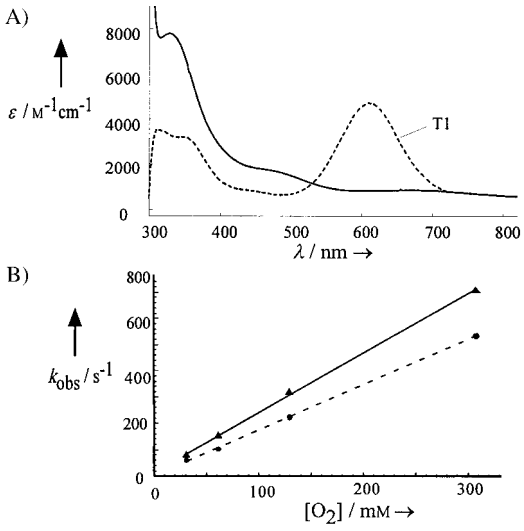

Figure 22. A) Absorption spectra of the peroxide intermediate (——) in T1Hg laccase and native intermediate (- - - -) in native laccase. The 600 nm band in the native intermediate is from the presence of the type 1 Cu center, B) rate of formation of the peroxide (▲, ——) and native intermediates (●, - - - -) as a function of O_2 concentration. Adapted from ref. [66]. The second-order rate constant for the peroxide intermediate is $2.2 \times 10^6\ M^{-1}s^{-1}$ and for native intermediate is $1.7 \times 10^6\ M^{-1}s^{-1}$.

360 nm assigned to the oxygen intermediate). Thus, in the native intermediate the dioxygen is at least one electron further reduced than in the T1Hg intermediate. However, as shown in Figure 22B, the native intermediate and the T1Hg oxygen intermediate have essentially the same rates of formation ($k \sim 2 \times 10^6\,\text{M}^{-1}\text{s}^{-1}$).[71] This similarity indicates that the formation of the T1Hg oxygen intermediate can be the rate-limiting step in the reduction of O_2 and that the rate of electron transfer from the distant type 1 through the >13 Å long Cys–His pathway to the trinuclear copper cluster is very fast ($>10^3\,\text{s}^{-1}$). Spectroscopy has shown (summarized in Section 4.2.1) that the T1Hg oxygen intermediate consists of a peroxy species bound to the trinuclear copper cluster and has a different geometric and electronic structure to that of oxy-hemocyanin. In Section 4.2.2, we extend these studies to define the nature of the native intermediate, which is shown to be a fully oxidized form of the enzyme and is different from the fully oxidized resting state. These studies lead to a proposal for the molecular mechanism of the four-electron reduction of dioxygen to water and insight into the reductive cleavage of the O–O bond (Section 4.2.3).

4.2.1. Peroxy Intermediate: Comparison to Oxy-hemocyanin

Results from isotope-ratio mass spectrometry (IRMS), show that both the O atoms from the O_2 molecule are present in the T1Hg oxygen intermediate, which indicates that the intermediate is a superoxo or peroxo species. These possibilities could be distinguished using the ligand-field region of the CD/MCD spectra (Section 4.1). Figure 23A shows that all the ligand-field transitions of the type 3 copper centers are present in the CD spectrum of the T1Hg intermediate, therefore both type 3 copper centers are oxidized. However, the low-temperature MCD spectrum of the intermediate (Figure 23B) exhibits no type 2 feature (consistent with the lack of a type 2 EPR signal) indicating that the type 2 copper is reduced. Two electrons have been transferred to O_2 from the type 3 copper centers, thus the intermediate is a peroxide species.[37]

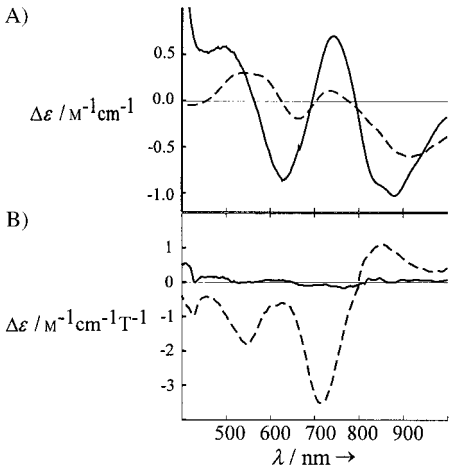

Figure 23. Comparison of the ligand-field transitions in the peroxide intermediate (——) and resting T1Hg laccase (- - - -). A) Ligand-field transitions of the type 3 Cu center, obtained by room-temperature CD and, B) ligand-field transitions of the type 2 Cu center, obtained by low-temperature MCD. Adapted from ref. [37].

SQUID magnetic-susceptibility measurements were used to define the magnetic interactions between the two oxidized type 3 copper centers of this peroxide intermediate. From saturation magnetization and Curie plots (referenced to the fully oxidized T1Hg derivative), the two oxidized type 3 centers of the peroxide intermediate were found to be strongly antiferromagnetically coupled with $-2J > 200\,\text{cm}^{-1}$. This exchange-coupling requires the presence of a bridging ligand between the two type 3 Cu^{II} centers. The bridging ligation was explored by X-ray absorption spectroscopy (XAS) of the T1Hg peroxy intermediate. The Fourier transform of the EXAFS spectrum of the intermediate has an intense outer-shell peak at a $\sim$3.4 Å (phase-shift corrected; Figure 24) which is not present in the oxidized resting (or reduced) trinuclear copper cluster. This result requires the presence of a tightly bound bridging ligand between two copper centers that cannot be the μ-hydroxide present in the oxidized trinuclear copper site (Figure 21B), since this does not have the favorable Debye–Waller factor required for the observation of an outer-shell peak. Thus, two copper centers of the peroxy intermediate of T1Hg laccase are tightly bridged together (Cu–Cu distance of 3.4 Å) by the peroxide.[37]

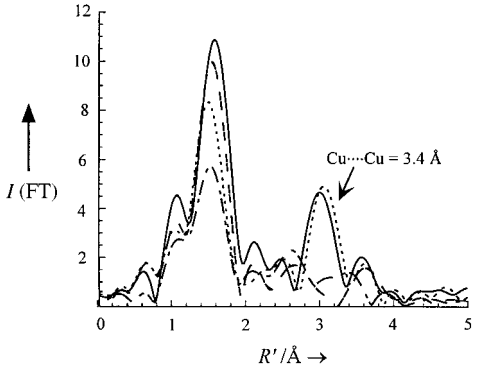

Figure 24. EXAFS spectra (I(FT) = intensity of the Fourier transformed signal) of oxidized T1Hg laccase (– – –), the peroxide intermediate (••••), the peroxide adduct (——), and reduced T1Hg laccase (•–•–). Reproduced from ref. [67].

The antiferromagnetism indicates that the two oxidized type 3 copper centers have a bridging ligand. The possibility of bridging between the type 3 and type 2 copper centers is more difficult to probe in the peroxy intermediate as the type 2 copper center is reduced. However, peroxide binds to the oxidized trinuclear copper cluster in the resting T1Hg derivative producing the peroxy adduct.[67] This adduct has the same intense outer-shell EXAFS peak as the T1Hg peroxy intermediate (Figure 24) indicating a similar peroxide bridging mode. However, in the peroxy adduct, the type 2 copper center is oxidized and paramagnetic and thus can be studied spectroscopically by low-temperature MCD (see Section 4.1), EPR, and other methods. From the EPR data in Figure 25A, the coordination environment of the type 2 Cu^{II} center

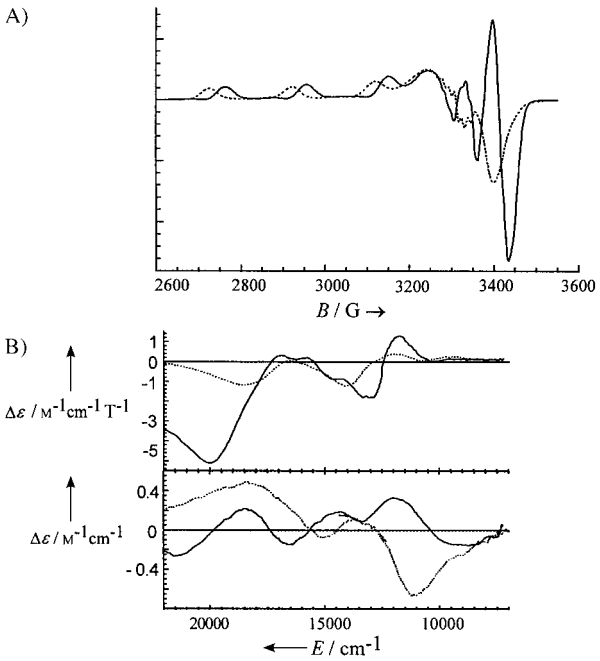

Figure 25. Comparison of the peroxide adduct of T1Hg laccase (——) and resting T1Hg laccase (- - - -). A) EPR and B) low-temperature MCD of the type 2 Cu center and room-temperature CD of the type 3 Cu center. Reproduced from ref. [67].

dramatically changes from rhombic to axial upon peroxide binding to the oxidized trinuclear Cu^{II} cluster. A ligand-field analysis indicates that the type 2 Cu^{II} site becomes four coordinate in the peroxy-bound form. This analysis is supported by the large change in the ligand-field transitions of the type 2 center in the low-temperature MCD spectrum (Figure 25B, top). In addition, there is a peroxide $\rightarrow Cu^{II}$ charge-transfer feature in the peroxide adduct at 400 nm, which has a large low-temperature MCD signal indicating that peroxide is bound to the type 2 Cu^{II} center. The changes in the ligand-field CD features (Figure 25B, bottom) and the fact that there is a peroxide $\rightarrow Cu^{II}$ charge-transfer transition in the absorption spectrum of the peroxide adduct with no associated low-temperature MCD feature (see reference [67]) requires that the peroxide also binds to the type 3 center thus forming a bridge between the type 2 and the type 3 copper centers.

The above studies lead to the two possible descriptions of the peroxide intermediate of the trinuclear copper cluster in the multicopper oxidases shown in Figure 26. In one model, the peroxide internally bridges the type 2 to the type 3 copper centers with the magnetic coupling between the oxidized

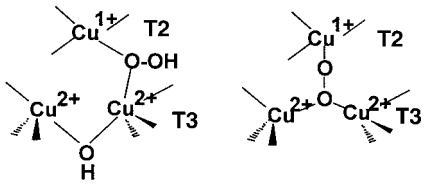

Figure 26. Possible structural models of the peroxide intermediate in the multicopper oxidases where the peroxide intermediate bridges the type 2 and type 3 Cu centers.

type 3 Cu^{II} centers arising from antiferromagnetic coupling through the peroxy bridge. Alternatively, the type 3 Cu^{II} centers could be linked by the hydroxide bridge which is present in the resting site (Figure 21B) and the peroxide could externally bridge the type 2 Cu^{I} and the type 3 Cu^{II} centers as hydroperoxide. Electronic-structure calculations are underway to distinguish between these possibilities. However, it is important to emphasize that both possibilities have a fundamentally different geometric and electronic structure than the μ-η^2:η^2 side-on peroxide bridged structure of oxy-hemocyanin (Figures 3 and 4). This difference can be seen from comparison of the charge-transfer spectra of the peroxide intermediate and oxy-hemocyanin (Figure 27). While the charge-transfer transition of the peroxy intermediate is comparably high in

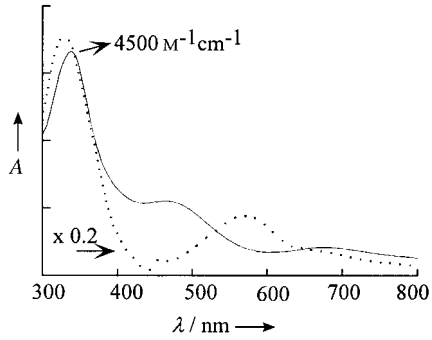

Figure 27. Comparison of the absorption spectra of the peroxide intermediate in T1Hg laccase (——) and the side-on peroxy site in oxy-hemocyanin (- - - -). The 330 nm peak in the oxy-hemocyanin spectrum is scaled down by on fifth to facilitate comparison.

energy at 340 nm, it has less than one fifth of the intensity of that of the oxy-hemocyanin. Such high energy but low intensity requires strong bonding interactions of the peroxide with nonchromophoric atoms (i.e. not Cu^{II}), either the proton in the μ-hydroperoxide arrangement or the type 2 Cu^{I} center in the μ-$(\eta^1)_3$ structure in Figure 26. The low charge-transfer intensity indicates a weak electron-donor interaction with the oxidized copper centers (in contrast to oxy-hemocyanin) which stabilizes the peroxide intermediate at the trinuclear copper-cluster site against the reversible loss of O_2. Further, the protonation of the peroxide (and/or its bonding interaction with the reduced type 2 copper) lowers the energy of the peroxide σ* orbital which activates it for the reductive cleavage of the O–O bond. This reaction is very slow in the peroxy intermediate of T1Hg laccase (0.0003 s^{-1} at pH 7.5) even though the peroxide is bridged to a reduced type 2 copper.[38] MCD studies have shown that the slow reductive cleavage of the peroxide intermediate in T1Hg generates a native intermediate-like species.[37] However, in the native enzyme the native intermediate is generated at a rate of $10^6\,M^{-1}s^{-1}$ (Figure 22B) indicating that the reduction of a peroxy species to form the native intermediate must be very fast ($>350\,s^{-1}$). The nature of the native intermediate is defined below where this difference in reactivity is found to reflect the one- versus two-electron reductive cleavage of the O–O bond.

4.2.2. Native Intermediate: Comparison to the Resting Enzyme

Figure 22 A shows the T1 copper center is oxidized in the native intermediate, thus O_2 must be at least one-electron further reduced than in the T1Hg peroxy intermediate. This combined with the facts that no EPR signal corresponding to type 2 centers is present and that a new broad EPR signal is observed (see below) which further broadens with the use of $^{17}O_2$ led researchers to describe the native intermediate as a three-electron reduced oxyl or hydroxyl species with the type 2 copper center still reduced.[35, 69] The oxidation state of the copper centers in the native intermediate could be directly determined by X-ray absorption edge studies,[72] where we have shown that there is a 1s →4p peak at 8984 eV characteristic of reduced but not oxidized copper. The X-ray edge of the native intermediate of laccase is superimposable with that of the fully oxidized resting enzyme indicating that all the copper centers are oxidized in the native intermediate (Figure 28 A).[73] Thus, O_2 is reduced by four electrons to the $H_2O/OH^-/O^{2-}$ level.[34] Further, the Fourier transform of the EXAFS spectrum of the native intermediate (Figure 28 B shows an outer-shell peak, which is not present in the resting site, that can only be fit to a Cu – Cu interaction at a distance of 3.3 Å.[73]

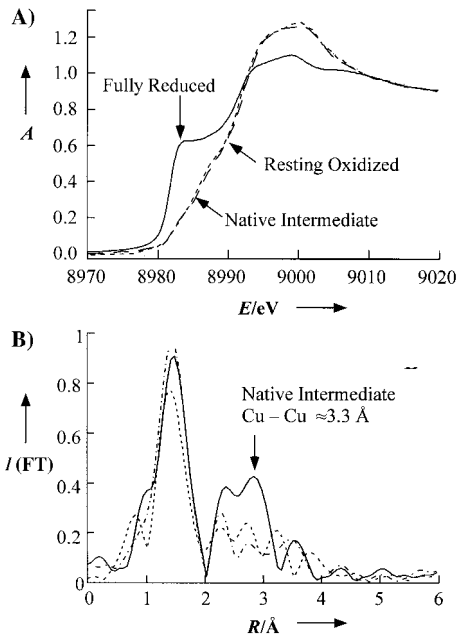

Figure 28. A) Cu_K-edge data for reduced (——), fully oxidized (– – –), and renormalized native intermediate (- - - -; corrected for unreacted reduced laccase); A = normalized absorption, B) nonphase-shift corrected Fourier transforms of the EXAFS data for reduced (•–•–), fully oxidized (- - - -), and native intermediate (——) forms of laccase; I(FT) = intensity of the Fourier transformed signal. Adapted from ref. [73].

While the native intermediate has a fully oxidized trinuclear copper cluster, it has a very different EPR signal from that of the resting oxidized trinuclear cluster, which exhibits the normal EPR signal of the localized type 2 Cu^{II} center (Figure 25 A).[35, 73, 74] The EPR signal of the native intermediate (Figure 29 A with the oxidized type 1 spectrum subtracted) is very broad with low g values including two below 2.00. From the frequency dependence of the g values the ground state has $S = ½$.[73] The EPR signal rapidly relaxes and cannot be observed above 20 K (Figure 29 B). This rapid relaxation suggests the presence of a low-lying excited state and from an Orbach analysis of the temperature dependence of the power saturation, the energy of this state could be estimated at $\sim 150\ cm^{-1}$ above the ground state (Figure 29 C).[73]

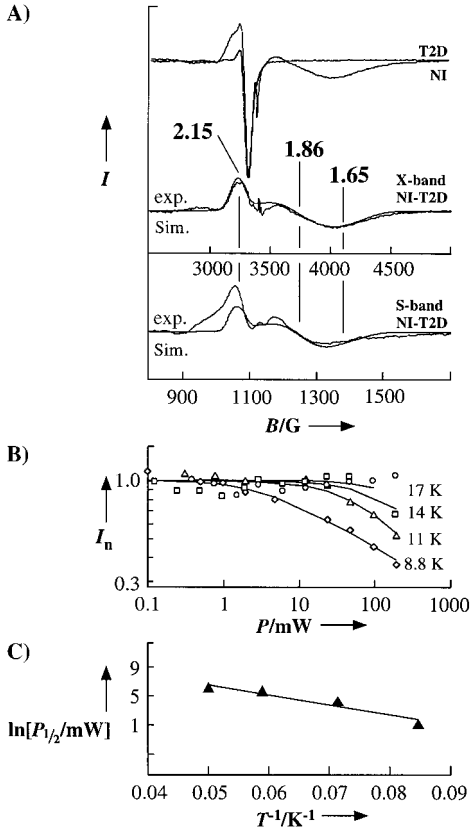

Figure 29. A) Top: the X-band EPR spectra of the native intermediate (NI) and T2D laccase at 200 mW and 10 K, bottom: the X-band and S-band EPR spectra measured T2D subtracted native intermediate (NI – T2D). Simultaneous simulations of the spectra giving g values of 2.15, 1.86, and 1.65 are included (Sim.), B) power saturation studies of the native intermediate. The normalized EPR intensities of the native intermediate at a resonance position around 4000 Gauss are plotted against microwave power varying from 0.1 to 200 mW at (◇) 8.8 K, (△) 11 K, (□) 14 K, and (○) 17 K, C) replot of the $\ln[P_{1/2}]$ against the inverse of temperature, which shows a linear response indicating a low-lying excited state at approximately 140 cm^{-1}. Adapted from ref. [73].

Further insight into the ground and excited states of the oxidized trinuclear copper cluster in the native intermediate could be obtained from the temperature and field dependence of its MCD spectrum. In addition to the 600 nm absorption feature of the type 1 center, the native intermediate exhibits absorption features at 365 and 318 nm (Figure 30 A), which correspond to oxo or hydroxo charge-transfer transitions to the Cu^{II} centers of the trinuclear copper cluster.[73] At low temperature these show a large derivative-shaped MCD signal (Figure 30 A, bottom).[34, 73] The field dependence of these MCD features at low temperature give a saturation

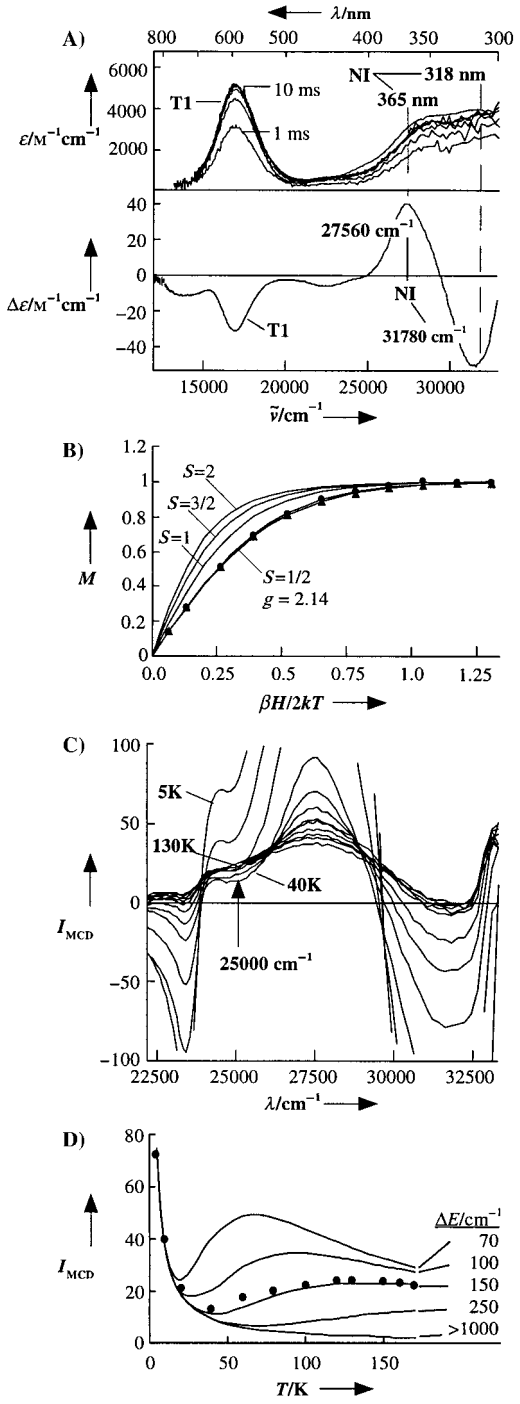

Figure 30. A) Top: formation of the native intermediate (NI) monitored using rapid scan stopped-flow absorption spectroscopy at pH 7.5 and 4 °C. The first scan is taken at 1.28 ms and each successive scan is taken every 2.56 ms up to 11.52 ms. Bottom: the low-temperature MCD spectrum of the native intermediate measured at 7 T and 1.8 K, B) saturation magnetization of the native intermediate MCD spectrum measured at 27560 cm^{-1} (▲) and 31780 cm^{-1} (●) at 1.8 K. Solid lines are simulations based on the different possible spin states indicated. M = normalized magnetization, C) the temperature dependence of the native intermediate MCD spectrum in expanded charge-transfer region (1.8–160 K at 7 T). Note that the MCD signal does not simply decrease as $1/T$; this indicates population of an excited state with a different MCD spectrum, D) the temperature dependence of the native intermediate MCD spectrum taken at 25000 cm^{-1} (●, arrow in part C). The signal intensity decreases between 5 K and 40 K but rises again at higher temperatures, 50–150 K. The solid lines are simulations with different excited-state splitting (best fit ca. 150 cm^{-1}). Adapted from ref. [73].

magnetization curve (Figure 30B) which can be described by a Brillouin function corresponding to an $S = ½$ ground state.[73] The temperature dependence of the high-field MCD spectrum is shown in Figure 30C for the charge-transfer region of the trinuclear copper cluster. For mononuclear $S = ½$ systems, the MCD signal simply decreases with increasing temperature (proportional to $1/T$). However, from the data in Figure 30 the spectra of the native intermediate *change* with increasing temperature indicating Boltzmann population of an excited state with a different MCD spectrum from that of the ground state. For example, the data taken at the 25000 cm^{-1} (arrow, Figure 30C) show that the MCD signal first decreases from 5 to 40 K and then increases with increasing temperature (Figure 30D). Fitting the energy for the excited state being thermally populated gives an energy of 150 cm^{-1}, in agreement with the Orbach analysis of the EPR data.[73]

Thus, the oxidized trinuclear copper cluster site in the native intermediate has an $S = ½$ ground state and a low-lying excited state at around 150 cm^{-1}. We now consider the exchange coupling associated with bridging-ligand interactions between the three Cu^{II} $S = ½$ ions which will reproduce these ground-state features. The exchange coupling of two Cu^{II} centers (Cu_a and Cu_b) associated with the bridging ligand gives a singlet ground state and triplet excited state split in energy by $2J$ (Figure 31). The third Cu^{II} $S = ½$ vector couples to this to produce an $S_{tot} = ½$ ground state ($|S = ½,0\rangle$) and $S_{tot} = ½$ and ⅜ excited states at $2J$. Allowing for a second bridging interaction between copper centers Cu_b and Cu_c splits the energy of the excited ½ and ⅜ states with the $|S = ½,1\rangle$ in Figure 31B being the state observed at

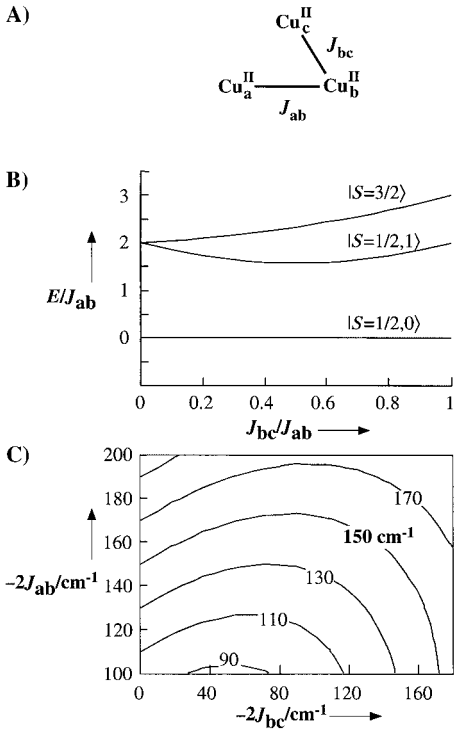

Figure 31. A) Scheme of two-bridge model, B) energy diagram of the two-bridge model as a function of the exchange-coupling ratio, C) solution space for the 150 cm^{-1} separation of the ground state and the first excited state as a function of the two exchange-coupling values based on the two bridge-model. Adapted from ref. [73].

$\sim 150\ cm^{-1}$. A search of the solution space giving an $|S=½,0\rangle/|S=½,1\rangle$ state splitting of $150\ cm^{-1}$ with two bridging ligands (Figure 31C) indicates that the maximum value of J that can be associated with either bridge is approximately $170\ cm^{-1}$.[73] However, the EXAFS data in Figure 28B show that there is a bridged Cu–Cu distance of 3.3 Å. Magneto-structural correlations have been developed for hydroxide-bridged Cu^{II} dimers,[75, 76] which show that at this distance the exchange coupling should be about $520\ cm^{-1}$. This value should be even larger for an oxo bridge (see below, Figure 32). To have an excited state at $150\ cm^{-1}$ with this large exchange coupling (required by the Cu–Cu distance), there must be a third bridge (between Cu_a and Cu_c) which would lead to spin frustration and lower the energy of the $|S=½,1\rangle$ excited state.

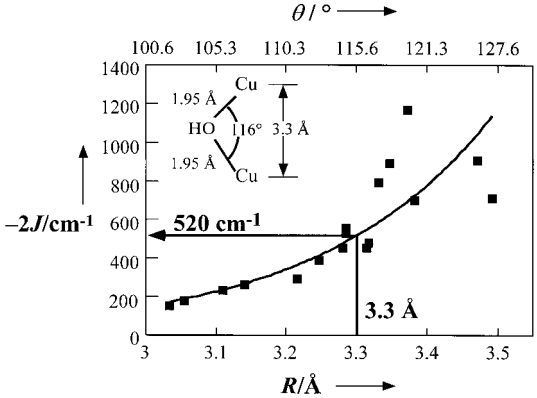

Figure 32. Magneto-structural correlation of the Cu–Cu distance R and the Cu-O-Cu angle (θ) with coupling constants for OH-bridged binuclear Cu^{II} model complexes. Note that there is a nonlinear relationship between the Cu-O-Cu angle and the Cu–Cu distance. Data taken from ref. [76].

Figure 33B presents the solution space giving an $|S=½,0\rangle/|S=½,1\rangle$ energy splitting of $150\ cm^{-1}$ as a function of the three different J values. Fixing $-2J_{ab}$ at $520\ cm^{-1}$ for the Cu–Cu distance of 3.3 Å, the other J values are also required to be large and within ⅔ of this value. The specific J values can be determined from the relative couplings of the three Cu^{II} $S=½$ centers of the trinuclear cluster to the ground $|S=½,0\rangle$ and excited $|S=½,1\rangle$ state wavefunctions; this was obtained experimentally from a comparison of the excited to ground state MCD spectra, where the former was obtained from the temperature dependence of the spectrum in Figure 30C.[73] From Figure 33D, the bands labeled ① correspond to charge-transfer transitions to a Cu^{II} center which change their MCD sign between the ground and excited state, while the band labeled ② goes from strong positive to weak positive and the band labeled ③ goes from weak positive to strong positive in the ground to excited state MCD spectrum. These behaviors reflect the coupling coefficients of the three Cu^{II} centers to the ground and excited $S=½$ states for specific values of $-2J$ (Figure 33C). (Bands ① are charge-transfer transitions to Cu^{II}_b, ② to Cu^{II}_c, and ③ to Cu^{II}_a.) Fitting the experimental MCD data in Figure 33D to Figure 33C gives the three J values which are included in Figure 33A and shows that the unusual spectra of the native intermediate are associated with a fully oxidized trinuclear copper cluster but with all three

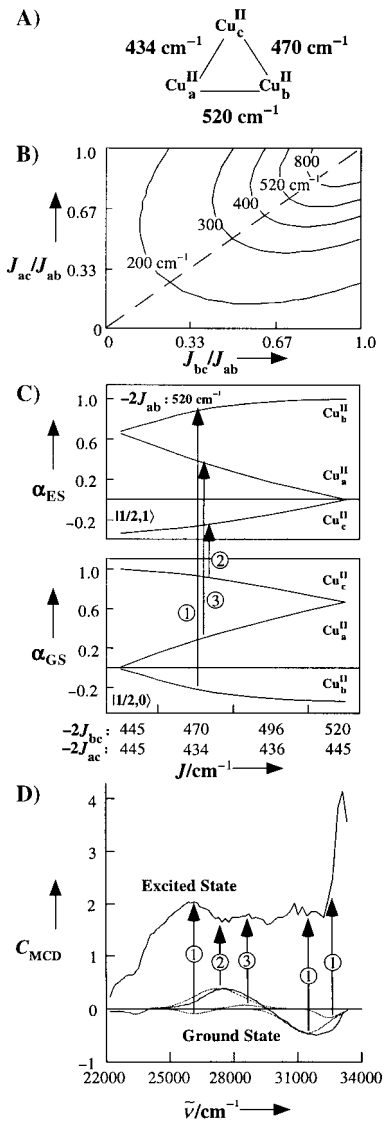

Figure 33. A) Three-bridge model with established coupling constants for the native intermediate, B) solution space for the first excited state at $150\ cm^{-1}$ as a function of the ratio of coupling constants with the third coupling constant fixed at the energy indicated, C) coupling coefficients of the individual copper centers of the trinuclear Cu^{II} cluster in the ground state and excited state wavefunctions; α_{ES} = excited state coefficient, α_{GS} = ground state coefficient (see ref. [73]), D) the ground and excited state MCD spectra of the native intermediate. Bands are grouped together (①, ②, and ③) according to their different temperature dependencies, which correlate with the change in coupling constants indicated in part (C). Gaussian simulation of the ground state spectrum is shown in gray. Adapted from ref. [73].

copper centers involved in strong bridging interactions.[73] This situation leads to the two possible structure models of the native intermediate (NI) shown in Figure 34 where the four-electron reduction of dioxygen has either produced two additional OH^- bridges or one μ_3-oxo bridge.

In summary, the studies of the native intermediate described above show that all four copper centers are oxidized and that this is a four-electron O^{2-}/OH^- product and not a three-electron O^-/OH intermediate. However, the native intermediate is different from the resting enzyme because all the copper centers of the oxidized trinuclear copper cluster

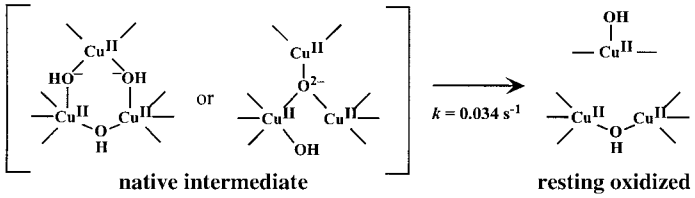

Figure 34. Structural model of the native intermediate, and its decay to the resting oxidized state.

are bridged. The decay of the native intermediate to form the resting enzyme is very slow ($k = 0.034\ s^{-1}$).[77] ^{18}O IRMS combined with ^{17}O EPR studies of the reaction of the reduced enzyme with labeled O_2, show that one oxygen atom of the O_2 unit is present in the resting enzyme. This atom is bound terminally to the type 2 copper center and lies outside the trinuclear cluster (Figure 34).[78, 79] Thus, the slow decay of the native intermediate to the resting oxidized enzyme is consistent with a large structural change that would be associated with the rearrangement of the oxygen atom, from the O_2 molecule, from inside to outside the cluster. Finally it should be emphasized that both the rate of decay of the native intermediate and the rate of reduction of the oxidized trinuclear copper cluster of the resting enzyme are too slow to be consistent with the catalytic turnover.[80–83] Alternatively, the reduction of the native intermediate is rapid indicating that this is the fully oxidized form of the enzyme which is active in catalysis.[7] It is possible that the bridge(s) to the type 2 copper center of the cluster couple this center into the electron-transfer pathway allowing rapid reduction by electrons entering at the type 1 copper center (through the Cys–His pathway to the type 3 center in Figure 1D). This possibility is under investigation.

4.2.3. Molecular Mechanism: Reductive Cleavage of the O–O Bond

The definition of the intermediates in the reduction of O_2 to H_2O in the multicopper oxidases leads to the molecular mechanism for this four-electron process given in Figure 35.

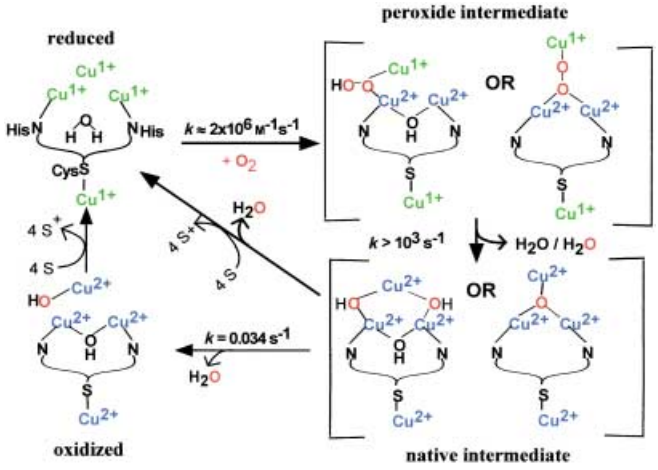

Figure 35. Molecular mechanism for the reduction of O_2 to H_2O in the multicopper oxidases.

The reduced enzyme reacts with dioxygen to generate a two-electron reduced peroxide intermediate with the peroxide bridging an oxidized type 3 copper pair and a reduced type 2 copper center. This peroxide intermediate is reduced in a second two-electron step, thus oxidizing the type 2 and the distant type 1 center to generate the "native intermediate" which is, in fact, an oxo or hydroxo product bridged between the oxidized type 3 and now oxidized type 2 copper centers of the trinuclear cluster. This intermediate is either rapidly reduced by substrate in the catalytic reaction, or, in the absence of substrate, slowly decays to the resting site which contains one oxygen atom of the O_2 terminally bound as H_2O to the type 2 copper. This rearrangement uncouples the trinuclear copper cluster and removes the resting enzyme from the catalytic cycle.

Thus, the reduction of O_2 to H_2O involves two, two-electron steps and from the kinetics shown in Figure 22B, the first step is rate determining and the second is very fast. It is important to note that the second step involves the reductive cleavage of the O–O bond and there is a large Franck–Condon barrier associated with this distortion. We were able to experimentally study this barrier through the temperature dependence of the decay of the peroxide intermediate in the T1Hg laccase, which involves the one-electron (electron from the reduced type 2 center) reductive cleavage of the O–O bond.[38] From the $k(^{16}O_2)/k(^{18}O_2)$ kinetic oxygen isotope effect of 1.10 ± 0.05, the rate-determining step in this reaction is O–O bond cleavage. The experimental barrier we find is quite large ($\sim 9\ kcal\,mol^{-1}$) which is consistent with a slow rate of decay ($3 \times 10^{-4}\ s^{-1}$). From the Marcus theory for electron transfer, the rate for this reduction should depend on the electronic-coupling matrix element (H_{DA}; D = donor, A = acceptor), the thermodynamic driving force (ΔG°), and the reorganization energy (λ). Since the peroxide in the T1Hg intermediate is bound to the type 2 copper center, H_{DA} should be large. The redox potential of the type 2 center in the resting enzyme is 0.37 V,[84] which is close to the E° for the one-electron reduction potential of H_2O_2 (0.38 V), and therefore ΔG° is small and the reaction is thermo-neutral. For an isoenergetic process, the reorganization energy associated with the cleavage of the O–O bond should be around one quarter of the dissociation energy of the bond,[85] which has been estimated to be between 34 and 50 $kcal\,mol^{-1}$ for peroxide.[86–88] This value predicts an activation energy of 8.5–12.5 $kcal\,mol^{-1}$ which is in good agreement with experiment. That the peroxide intermediate is not observed in the native enzyme indicates that the conversion of the peroxide intermediate into the native intermediate is fast relative to its formation (the rate of formation of the peroxide intermediate in T1Hg is $2 \times 10^6\ M^{-1}\,s^{-1}$). Kinetic modeling of the general reaction scheme [Eq. (1)], places a lower limit of $\sim 350\ s^{-1}$ on

$$\text{reduced enzyme} + O_2 \longrightarrow \text{peroxide intermediate} \longrightarrow \text{native intermediate} \longrightarrow \text{resting enzyme} \quad (1)$$

the conversion of the peroxide intermediate into the native intermediate which is $\sim 10^6$ times faster than the one-electron reductive cleavage of the O–O bond in the T1Hg intermediate.[38]

However, in the native enzyme this reaction involves a two-electron transfer, one electron from the type 2 and one from the type 1 copper centers (through the Cys–His pathway), which produces the fully oxidized native intermediate. The E° of the type 1 center is 0.39 V which is similar to that of the type 2 center.[84] Importantly, the potential for two-electron reduction of peroxide is 1.37 V which is one volt ($\sim$46 kcal mol^{-1} for $n=2$ in the Nernst equation) more favorable than the one-electron reduction. This adds a large thermodynamic driving force which greatly lowers the activation barrier (to around 1 kcal mol^{-1}). The difference in activation energy for the 1e$^-$ versus 2e$^-$ reductive cleavage of peroxide is shown in Figure 36. This large difference in activation energy would lead to a 10^7-fold increase in the peroxide reduction rate in the native enzyme, consistent with experiment and the reaction mechanism in Figure 35; O_2 is reduced in two two-electron steps, the second being very rapid because of the large driving force for this reaction.

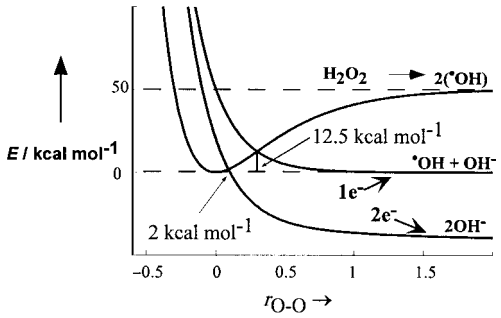

Figure 36. Potential-energy surfaces for the one versus two-electron reductive cleavage of the O–O bond of peroxide. Morse potentials are used to model the reactant (H_2O_2) and product (1e$^-$ and 2e$^-$ cleavage of H_2O_2). The product curve for the 2e$^-$ reductive cleavage is shifted to lower energy by 46 kcal mol^{-1}.

Figure 36 provides general insight into strategies for the reductive cleavage of O–O bonds in biology. Because of the large Franck–Condon barrier associated with this cleavage, there has to be a large thermodynamic driving force for the rapid rate required by most biological processes. This can be achieved either by the stability of the M=O product formed in the one-electron process (e.g. Fe^{IV}=O) or by the one volt more favorable two-electron reduction of peroxide.

5. Summary and Outlook

The unique spectral features of copper/dioxygen intermediates are generally understood and reflect new electronic structures which make major contributions to reactivity. These studies have defined geometric- and electronic-structure/function correlations and led to molecular mechanisms for the reversible binding of oxygen by hemocyanin, oxygen activation by tyrosinase, and the four-electron reduction of oxygen to water by the multicopper oxidases. They have further provided general insight into the reductive cleavage of the O–O bond, an important problem in many areas of biology. Fundamental questions still remain including the nature of the substrate interactions in the different enzymes, how mutations perturb the active sites and change their reactivity, the nature of the oxygen intermediates in the noncoupled binuclear copper enzymes, and in the biosynthesis of the organic cofactors, how the oxygen intermediates in the multicopper oxidases relate to those in cytochrome c oxidase, and how the type 1 copper center couples to the trinuclear copper cluster through the Cys–His pathway in the multicopper oxidases. We look forward to many exciting new insights in the field of copper/O_2 chemistry in the years ahead.

E.I.S. thanks his collaborators and past students as indicated in the references cited for their outstanding contributions to this field. This research was generously funded by the National Institute of Health (DK31450). The following fellowships are gratefully acknowledged: Peng Chen, Gerhard Casper Stanford Graduate Fellowship, Markus Metz, DAAD Postdoctoral Fellowship, Amy Palmer, Franklin Veatch Memorial Fellowship.

Received: April 2, 2001 [A 462]

[1] R. H. Holm, P. Kennepohl, E. I. Solomon, *Chem. Rev.* **1996**, *96*, 2239.
[2] I. E. Marko, M. Tsukazaki, P. R. Giles, S. M. Brown, C. J. Urch, *Angew. Chem.* **1997**, *109*, 2297; *Angew. Chem. Int. Ed. Engl.* **1997**, *36*, 2208.
[3] E. I. Solomon, P. M. Jones, J. A. May, *Chem. Rev.* **1993**, *93*, 2623.
[4] J. B. Reitz, E. I. Solomon, *J. Am. Chem. Soc.* **1998**, *120*, 11467.
[5] E. I. Solomon, F. Tuczek, D. E. Root, C. A. Brown, *Chem. Rev.* **1994**, *94*, 827.
[6] J. P. Klinman, *Chem. Rev.* **1996**, *96*, 2541.
[7] E. I. Solomon, U. M. Sundaram, T. E. Machonkin, *Chem. Rev.* **1996**, *96*, 2563.
[8] S. Ferguson-Miller, G. T. Babcock, *Chem. Rev.* **1996**, *96*, 2889.
[9] A. Messerschmidt, R. Ladenstein, R. Huber, M. Bolognesi, L. Avigliano, R. Petruzzelli, A. Rossi, A. Finazzi-Agro, *J. Mol. Biol.* **1992**, *224*, 179.
[10] T. Klabunde, C. Eicken, J. C. Sacchettini, B. Krebs, *Nat. Struct. Biol.* **1998**, *5*, 1084.
[11] V. Kumar, D. M. Dooley, H. C. Freeman, J. M. Guss, I. Harvey, M. A. McGuirl, M. C. J. Wilce, V. M. Zubak, *Structure* **1996**, *4*, 943.
[12] B. Hazes, K. A. Magnus, C. Bonaventura, J. Bonaventura, Z. Dauter, K. H. Kalk, W. G. Hol, *Protein Sci.* **1993**, *2*, 597.
[13] N. Ito, S. E. V. Phillips, C. Stevens, Z. B. Ogel, M. J. McPherson, J. N. Keen, K. D. S. Yadav, P. F. Knowles, *Nature* **1991**, *350*, 87.
[14] K. A. Magnus, B. Hazes, H. Ton-That, C. Bonaventura, J. Bonaventura, W. G. J. Hol, *Proteins: Struct. Funct. Genet.* **1994**, *19*, 302.
[15] S. T. Prigge, A. S. Kolhekar, B. A. Eipper, R. E. Mains, L. M. Amzel, *Science* **1997**, *278*, 1300.
[16] S. T. Prigge, A. S. Kolhekar, B. A. Eipper, R. E. Mains, L. M. Amzel, *Nat. Struct. Biol.* **1999**, *6*, 976.
[17] P. F. Knowles, D. M. Dooley, *Met. Ions Biol. Syst.* **1994**, *30*, 361.
[18] D. M. Dooley, D. E. Brown, H. C. Freeman, J. M. Guss, H. Matsunami, W. S. McIntire, C. E. Ruggiero, K. Tanizawa, M. Wilce, H. Yamaguchi, *FASEB J.* **1997**, *11*, 79.
[19] N. J. Blackburn, F. C. Rhames, M. Ralle, S. Jaron, *J. Biol. Inorg. Chem.* **2000**, *5*, 341.
[20] S. Jaron, N. J. Blackburn, *Biochemistry* **1999**, *38*, 15086.
[21] N. Kitajima, K. Fujisawa, Y. Moro-oka, *J. Am. Chem. Soc.* **1989**, *111*, 8975.
[22] R. S. Himmelwright, N. C. Eickman, C. D. LuBien, K. Lerch, E. I. Solomon, *J. Am. Chem. Soc.* **1980**, *102*, 7339.
[23] J. A. Halfen, S. Mahapatra, E. C. Wilkinson, S. Kaderli, V. G. Young, Jr., L. Que, Jr., A. D. Zuberbühler, W. B. Tolman, *Science* **1996**, *271*, 1397.
[24] P. K. Ross, E. I. Solomon, *J. Am. Chem. Soc.* **1990**, *112*, 5871.

[25] M. J. Henson, P. Mukherjee, D. E. Root, T. D. P. Stack, E. I. Solomon, *J. Am. Chem. Soc.* **1999**, *121*, 10332.
[26] P. Chen, K. Fujisawa, E. I. Solomon, *J. Am. Chem. Soc.* **2000**, *122*, 10177.
[27] D. E. Wilcox, A. G. Porras, Y. T. Hwang, K. Lerch, M. E. Winkler, E. I. Solomon, *J. Am. Chem. Soc.* **1985**, *107*, 4015.
[28] M. D. Allendorf, D. J. Spira, E. I. Solomon, *Proc. Natl. Acad. Sci. USA* **1985**, *82*, 3063.
[29] H. H. T. Nguyen, A. K. Shiemke, S. J. Jacobs, B. J. Hales, M. E. Lidstrom, S. I. Chan, *J. Biol. Chem.* **1994**, *269*, 14995.
[30] D. J. Kosman, R. Hassett, D. S. Yuan, J. McCracken, *J. Am. Chem. Soc.* **1998**, *120*, 4037.
[31] Note that herein we reserve the term T3Cu for the hydroxo bridged binuclear Cu component of the trinuclear Cu cluster. This has a different geometric and electronic structure from the coupled binuclear Cu sites in hemocyanin, tyrosinase, and catechol oxidase (sometimes also called T3 in the literature).
[32] I. Zaitseva, V. Zaitsev, G. Card, K. Moshov, B. Bax, A. Ralph, P. Lindley, *J. Biol. Inorg. Chem.* **1996**, *1*, 15.
[33] L.-E. Andréasson, R. Brändén, B. G. Malmström, T. Vanngard, *FEBS Lett.* **1973**, *32*, 187.
[34] P. A. Clark, E. I. Solomon, *J. Am. Chem. Soc.* **1992**, *114*, 1108.
[35] R. Aasa, R. Brändén, J. Deinum, B. G. Malmström, B. Reinhammar, T. Vanngard, *FEBS Lett.* **1976**, *61*, 115.
[36] M. M. Morie-Bebel, M. C. Morris, J. L. Menzie, D. R. McMillin, *J. Am. Chem. Soc.* **1984**, *106*, 3677.
[37] W. Shin, U. M. Sundaram, J. L. Cole, H. H. Zhang, B. Hedman, K. O. Hodgson, E. I. Solomon, *J. Am. Chem. Soc.* **1996**, *118*, 3202.
[38] A. E. Palmer, S.-K. Lee, E. I. Solomon, *J. Am. Chem. Soc.* **2001**, *123*, 6591.
[39] E. I. Solomon, M. J. Baldwin, M. D. Lowery, *Chem. Rev.* **1992**, *92*, 521.
[40] J. E. Pate, R. W. Cruse, K. D. Karlin, E. I. Solomon, *J. Am. Chem. Soc.* **1987**, *109*, 2624.
[41] N. C. Eickman, R. S. Himmelwright, E. I. Solomon, *Proc. Natl. Acad. Sci. USA* **1979**, *76*, 2094.
[42] T. B. Freedman, J. S. Loehr, T. M. Loehr, *J. Am. Chem. Soc.* **1976**, *98*, 2809.
[43] E. I. Solomon, D. M. Dooley, R. H. Wang, H. B. Gray, M. Cerdonio, F. Mogno, G. L. Romani, *J. Am. Chem. Soc.* **1976**, *98*, 1029.
[44] P. K. Ross, E. I. Solomon, *J. Am. Chem. Soc.* **1991**, *113*, 3246.
[45] M. J. Baldwin, D. E. Root, J. E. Pate, K. Fujidawa, N. Kitajima, E. I. Solomon, *J. Am. Chem. Soc.* **1992**, *114*, 10421.
[46] A. D. Becke, *J. Chem. Phys.* **1993**, *98*, 5648.
[47] T. H. J. Dunning, P. J. Hay in *Modern Theoretical Chemistry*, *Vol. 3* (Ed.: H. F. Schaefer III), Plenum, New York, **1976**, p. 1.
[48] P. J. Hay, W. R. Wadt, *J. Chem. Phys.* **1985**, *82*, 270.
[49] P. J. Hay, W. R. Wadt, *J. Chem. Phys.* **1985**, *82*, 299.
[50] W. R. Wadt, P. J. Hay, *J. Am. Chem. Soc.* **1985**, *82*, 284.
[51] M. E. Casida, *Recent Adv. Comput. Chem.* **1995**, *1*, 155.
[52] R. E. Stratmann, G. E. Scuseria, M. J. Frisch, *J. Chem. Phys.* **1998**, *109*, 8218.
[53] M. Metz, E. I. Solomon, *J. Am. Chem. Soc.* **2001**, *123*, 4938.
[54] M. Brouwer, C. Bonaventura, J. Bonaventura, *Biochemistry* **1978**, *17*, 2148.
[55] A. Berces, *Inorg. Chem.* **1997**, *36*, 4831.
[56] A. Berces, *Int. J. Quantum Chem.* **1997**, *65*, 1077.
[57] K. D. Karlin, J. C. Hayes, Y. Gultneh, R. W. Cruse, J. W. McKown, J. P. Hutchinson, J. Zubieta, *J. Am. Chem. Soc.* **1984**, *106*, 2121.
[58] E. Pidcock, H. V. Obias, C. X. Zhang, K. D. Karlin, E. I. Solomon, *J. Am. Chem. Soc.* **1998**, *120*, 7841.
[59] E. Pidcock, H. V. Obias, M. Abe, H.-C. Liang, K. D. Karlin, E. I. Solomon, *J. Am. Chem. Soc.* **1999**, *121*, 1299.
[60] D. E. Root, M. Mahroof-Tahir, K. D. Karlin, E. I. Solomon, *Inorg. Chem.* **1998**, *37*, 4838.
[61] P. P. Paul, Z. Tyeklar, R. R. Jacobson, K. D. Karlin, *J. Am. Chem. Soc.* **1991**, *113*, 5322.
[62] P. Chen, E. I. Solomon, *J. Inorg. Biochem.*, in press.
[63] D. J. Spira-Solomon, M. D. Allendorf, E. I. Solomon, *J. Am. Chem. Soc.* **1986**, *108*, 5318.
[64] J. L. Cole, G. O. Tan, E. K. Yang, K. O. Hodgson, E. I. Solomon, *J. Am. Chem. Soc.* **1990**, *112*, 2243.
[65] V. Ducros, A. M. Brzozowski, K. S. Wilson, S. H. Brown, P. Østergaard, P. Schneider, D. S. Yaver, A. H. Pedersen, G. J. Davies, *Nat. Struct. Biol.* **1998**, *5*, 310.
[66] J. L. Cole, P. A. Clark, E. I. Solomon, *J. Am. Chem. Soc.* **1990**, *112*, 9534.
[67] U. M. Sundaram, H. H. Zhang, B. Hedman, K. O. Hodgson, E. I. Solomon, *J. Am. Chem. Soc.* **1997**, *119*, 12525.
[68] M. Metz, E. I. Solomon, unpublished results.
[69] R. Aasa, R. Brändén, J. Deinum, B. G. Malmström, B. Reinhammar, T. Vanngard, *Biochem. Biophys. Res. Commun.* **1976**, *70*, 1204.
[70] L. E. Andréasson, R. Brändén, B. Reinhammar, *Biochim. Biophys. Acta* **1976**, *438*, 370.
[71] J. L. Cole, D. P. Ballou, E. I. Solomon, *J. Am. Chem. Soc.* **1991**, *113*, 8544.
[72] L. S. Kau, D. J. Spira-Solomon, J. E. Pennerhahn, K. O. Hodgson, E. I. Solomon, *J. Am. Chem. Soc.* **1987**, *109*, 6433.
[73] S.-K. Lee, S. D. George, W. E. Antholine, B. Hedman, K. O. Hodgson, E. I. Solomon, *J. Am. Chem. Soc.*, submitted.
[74] H. W. Huang, T. Sakurai, S. Maritano, A. Marchesini, S. Suzuki, *J. Inorg. Biochem.* **1999**, *75*, 19.
[75] V. H. Crawford, H. W. Richardson, J. R. Wasson, D. J. Hodgson, W. E. Hatfield, *Inorg. Chem.* **1976**, *15*, 2107.
[76] S. S. Tandon, L. K. Thompson, M. E. Manuel, J. N. Bridson, *Inorg. Chem.* **1994**, *33*, 5555.
[77] L.-E. Andréasson, B. Reinhammar, *Biochim. Biophys. Acta* **1976**, *445*, 579.
[78] R. Brändén, J. Deinum, *FEBS Lett.* **1977**, *73*, 144.
[79] R. Brändén, J. Deinum, M. Coleman, *FEBS Lett.* **1978**, *89*, 180.
[80] O. Farver, I. Pecht, *Proc. Natl. Acad. Sci. USA* **1992**, *89*, 8283.
[81] P. Kyritsis, A. Messerschmidt, R. Huber, G. A. Salmon, A. G. Sykes, *J. Chem. Soc. Dalton Trans.* **1993**, 731.
[82] T. E. Meyer, A. Marchesini, M. A. Cusanovich, G. Tollin, *Biochemistry* **1991**, *30*, 4619.
[83] L.-E. Andréasson, B. Reinhammar, *Biochim. Biophys. Acta* **1979**, *568*, 145.
[84] B. R. M. Reinhammar, *Biochim. Biophys. Acta* **1972**, *275*, 245.
[85] J.-M. Savéant, *Adv. Electron Transfer Chem.* **1994**, *4*, 53.
[86] A. C. Baldwin in *The Chemistry of Peroxides* (Ed.: S. Patai), Wiley, New York, **1983**, p. 97.
[87] R. D. Bach, P. Y. Ayala, H. B. Schlegel, *J. Am. Chem. Soc.* **1996**, *118*, 12758.
[88] X. Luo, P. R. Flemming, T. R. Rizzo, *J. Chem. Phys.* **1992**, *96*, 5659.